PHILOSOPHICAL TRANSACTIONS OF THE ROYAL SOCIETY A MATHEMATICAL, PHYSICAL & ENGINEERING SCIENCES

Baroclinic Waves in a Rotating Fluid Subject to Internal Heating

R. Hide and P. J. Mason

Phil. Trans. R. Soc. Lond. A 1970 **268**, 201-232
doi: 10.1098/rsta.1970.0073

BAROCLINIC WAVES IN A ROTATING FLUID SUBJECT TO INTERNAL HEATING

By R. HIDE and P. J. MASON
Geophysical Fluid Dynamics Laboratory, Meteorological Office, Bracknell, Berkshire

(*Communicated by J. S. Sawyer, F.R.S.—Received* 16 *February* 1970)

CONTENTS

Free thermal convection in a vertical rotating fluid annulus subject to axisymmetric heating and cooling applied at the side-walls has been the subject of extensive previous studies, one of the principal findings of which is that four distinct types of flow are possible, each characteristic of definite ranges of impressed experimental conditions. Three of these flow types are characterized by departures from axial symmetry and arise when the basic axisymmetric flow is 'baroclinically unstable'; they comprise 'baroclinic waves' of varying degrees of complexity (steady waves, waves subject to periodic fluctuations in form, amplitude and/or wavenumber ('vacillation') and waves subject to irregular non-periodic fluctuations).

The present paper reports an experimental and theoretical study of effects associated with the introduction of heat throughout the body of the fluid (rather than via one of the side-walls) and removal via the inner side-wall, the outer side-wall, or both side-walls simultaneously. The experiments show that the principal characteristics of the flow are fairly insensitive to the radial dependence of heating and cooling (upon which, for example, the horizontal shear of the basic axisymmetric flow depends), thereby strengthening the basis of the application to large-scale geophysical and astrophysical systems of theoretical ideas stemming from the laboratory work. Just as previous experiments have shown that the

Vol. 268. A. 1186. (Price 17*s*.; U.S. $2.20) 15 [Published 12 November 1970

presence of an inner wall does not preclude the occurrence of *irregular* baroclinic waves, one of the present experiments shows that the *absence* of an inner wall does not preclude the occurrence of *steady* baroclinic waves (thus refuting a certain conjecure which seems to have gained widespread acceptance among meteorologists). Determinations have been made of the general form of the flow pattern, top-surface flow velocities, total heat transfer and the transition between axisymmetric flow and baroclinic waves, and the results interpreted, where possible, in terms of theoretical ideas. The experiments provide striking support for a simple theoretical model that treats the jet stream associated with the baroclinic waves as a quasi-geostrophic detached thermal boundary layer.

1. Introduction

This paper reports experiments on thermal convection in a vertical rotating fluid annulus subject to internal heating (produced by the well-known technique of passing an a.c. current through the fluid), heat being removed from the convection chamber via the inner side-wall of

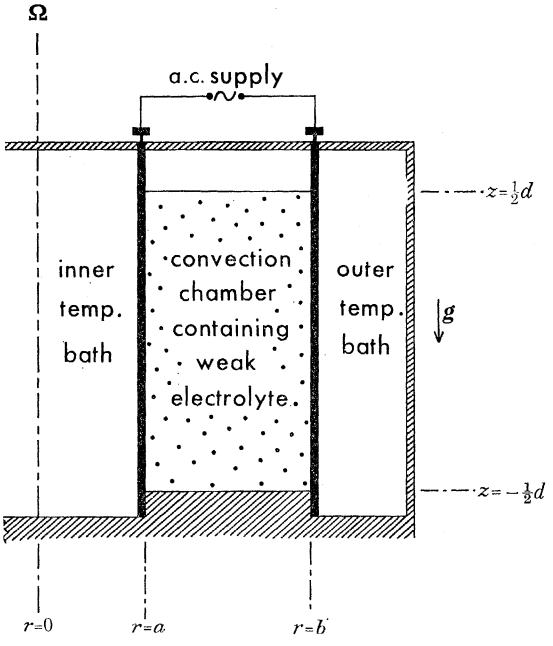

FIGURE 1. Schematic diagram illustrating rotating annulus of liquid. (r, ϕ, z) are cylindrical polar coordinates of a general point fixed in a frame moving with the apparatus, which rotates uniformly with angular velocity $\boldsymbol{\Omega}$ about a vertical axis relative to the laboratory (inertial) frame, and $\boldsymbol{g} = (0, 0, -g)$ is the acceleration of gravity. The liquid occupies the region $a < r < b$ and $-\frac{1}{2}d < z < \{d[\frac{1}{2}+\Omega^2(r^2-\frac{1}{2}(b^2+a^2)/2gd)]$ or $\frac{1}{2}d\}$ depending on whether the upper surface was free or in contact with a rigid lid in $z = \frac{1}{2}d$. In all the experiments, $\Omega^2(r^2-\frac{1}{2}(b^2+a^2))/2gd$ was so much less than unity that no primary effects due to the curvature of the upper surface occurred.

Internal heating was accomplished by passing an alternating electric current through the fluid in the convection chamber and wall heating was accomplished by means of one of the temperature baths. Cooling in all cases took place via one or both of the side-walls, each in contact with one of the temperature baths. Care was taken to ensure that the temperature field thus impressed on the fluid was axisymmetric and (by preventing heat losses via the upper and lower bounding surfaces) independent of z. The impressed temperature fields in each of two cases of wall heating and three cases of internal heating are illustrated in figure 3.

the annulus, the outer side-wall, or both inner and outer side-walls simultaneously (see figure 1). The investigation was carried out not only for its intrinsic interest but because of its bearing on the theoretical interpretation of the results of previous laboratory studies of wall-heated systems. As these previous studies are quite extensive and difficult to summarize succinctly here, it will

be convenient to refer frequently in what follows to a recent review article (Hide 1970, hereafter cited as Rev.), where a comprehensive bibliography can be found.

Work with wall-heated systems has shown that even when great care is taken to ensure that the apparatus is geometrically and physically symmetric about the axis of rotation, under certain conditions the ensuing hydrodynamical flow is non-axisymmetric (see tables 1 and 2 and

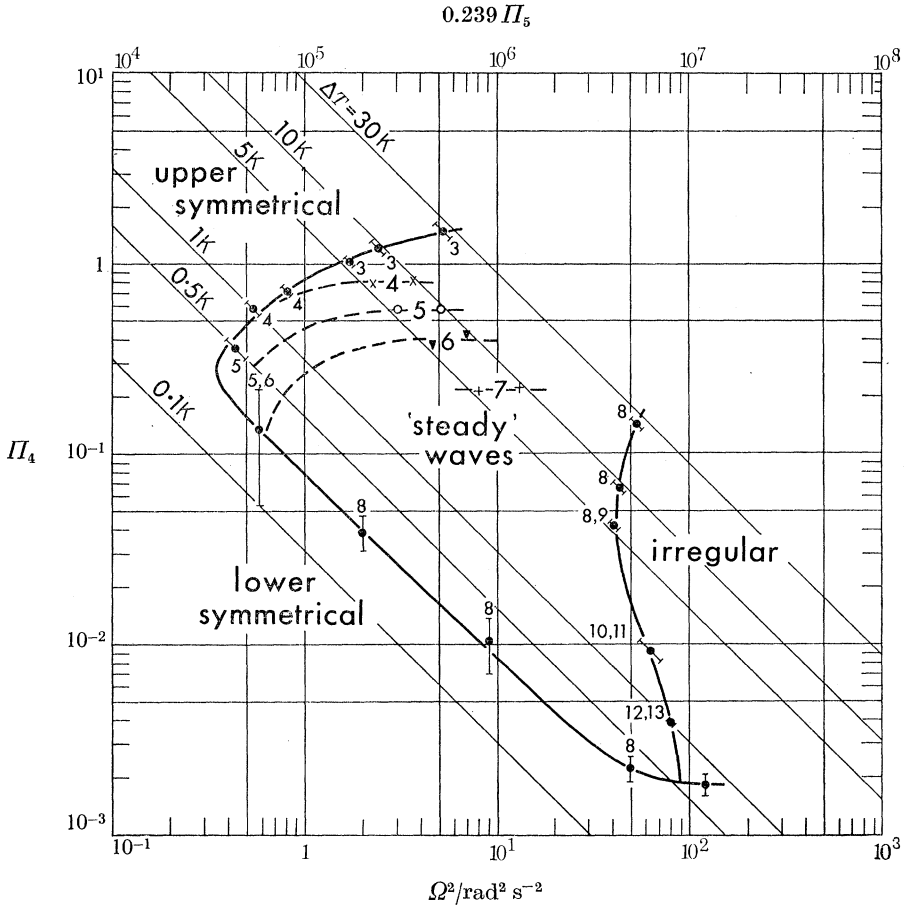

FIGURE 2. Typical régime diagram for wall-heated systems (after Fowlis & Hide 1965) illustrating the conditions under which axisymmetric flow, steady waves (with wavenumber ranging in this case from 3 to 13) and irregular flow occur: cf. figure 5.

$$\Pi_4 \equiv g\alpha\,|T_b - T_a|\,d/\Omega^2(b-a)^2 \quad \text{and} \quad \Pi_5 \equiv 4\Omega^2(b-a)^5/\nu^2 d \quad \text{(see table 2)}.$$

[This diagram was drawn for $a = 3.48\,\text{cm}$, $b = 6.02\,\text{cm}$, $d = 10.0\,\text{cm}$, $\nu = 1.01 \times 10^{-2}\,\text{cm}^2\,\text{s}^{-1}$, $\bar{\rho} = 0.998\,\text{g}\,\text{cm}^{-3}$. Upper surface: free; $\Pi_2 = 0.535$; $\Pi_3 = 4.82 \times 10^{-4}$ to 1.49×10^{-1}; $\Pi_6 = 7.9$; $\Pi_7 = 3.4 \times 10^{-4}$ to 8.54×10^{-2}; $\Pi_8 = 1.12 \times 10^6$ to 3.46×10^8. The upper transition depends mainly on Π_4 and Π_5; the lower transition occurs close to the line $\log_{10}(\Pi_4 \Pi_6) = -(0.864 \pm 0.043)\log_{10}(\Pi_2 \Pi_5) + (5.05 \pm 0.30)$.]

figure 2). Evidently the non-axisymmetric motions are fully developed 'baroclinic waves' (see Rev.), which arise when the basic axisymmetric flow is 'baroclinically unstable' to non-axisymmetric wave-like perturbations. 'Sloping convection' is a term which has been used to describe the motions in baroclinic waves, because typical trajectories of individual fluid elements are tilted at an angle to the horizontal that is comparable with but less than the slope of the isotherms. Baroclinic waves evidently underlie a number of natural phenomena occurring in stably stratified fluids, and interest in their properties has been shown not only by fluid

dynamicists but also by meteorologists, oceanographers and astrophysicists (see Rev.; Ward 1965; Lorenz 1967).

The theory of baroclinic instability and of the properties of small-amplitude baroclinic waves was first discussed by dynamical meteorologists, in their attempts to identify and understand the major potential-energy releasing eddies (the cyclones) in mid-latitudes. Theoretical studies of

TABLE 1. SOME DEFINITIONS

	symbol	definition
(1)	(r, ϕ, z)	cylindrical polar coordinates of general point in rotating system (see figure 1)
(2)	t	time
(3)	$\boldsymbol{g} = (0, 0, -g)$	acceleration of gravity, g taken as $9.81\,\mathrm{m\,s^{-2}}$
(4)	$\boldsymbol{\Omega} = (0, 0, \Omega)$	uniform angular velocity of rotation of apparatus
(5)	a, b	$a \leqslant r \leqslant b$ is horizontal extent of liquid in annular convection chamber
(6)	d	volume of liquid in convection chamber is $\pi(b^2-a^2)\,d$
(7)	$T(r, \phi, z, t)$	temperature at point (r, ϕ, z) at time t
(8)	$\rho = \rho(T)$	density at temperature T of liquid used in convection chamber
(9)	$\eta = \eta(T)$	coefficient of viscosity of liquid, usually strongly temperature dependent
(10)	$\nu = \nu(T)$	kinematic viscosity
(11)	$c = c(T)$	specific heat of liquid (depends only weakly on T)
(12)	$\chi = \chi(T)$	thermal conductivity of liquid (depends only weakly on T)
(13)	$\kappa = \kappa(T)$	thermometric conductivity $\equiv \chi/\rho c$
(14)	$\overline{T}$	mean temperature of liquid
(15)	P	rate at which internal heat is supplied, electrically, to fluid
(16)	$T_a,\ T_b$	$T(r=a), \quad T(r=b)$
(17)	$\Delta T_{\max}$	temperature difference between the warmest and cooled points in the convecting fluid (see note 1)
(18)	$T_{\sqrt{(ab)}}$	average value of T over the surface $r = \sqrt{(ab)}$
(19)	$\Delta\rho_{\max}$	$\rho(\overline{T}-\frac{1}{2}\Delta T_{\max}) - \rho(\overline{T}+\frac{1}{2}\Delta T_{\max})$
(20)	$\overline{\rho}, \overline{\nu}, \overline{\kappa}, \overline{c}$	$\rho(\overline{T}), \nu(\overline{T}), \kappa(\overline{T}), c(\overline{T})$ (see note 2)
(21)	$\sigma_z \Delta T_{\max}$	d times the mean vertical temperature gradient in the convecting liquid (see equation (3.2))

Note 1. $\Delta T_{\max} = |T_b - T_a|$ in the case of wall heating, but not otherwise.

Note 2. A *complete* list of all the quantities required to specify the system fully (cf. Fowlis & Hide 1965) includes parameters specifying the thermal properties of all the bounding surfaces, the surface tension and its variation with T, the range of variation of ν, κ and c and the form of the radial variation of the heating rate per unit volume (see text).

TABLE 2. SOME DIMENSIONLESS PARAMETERS

symbol	definition	range
Π_1	$(b-a)/\frac{1}{2}(b+a)$	1.98–0.40
Π_2	$d/(b-a)$	4.23–1.34
Π_3	$\Omega^2(b^2-a^2)/2gd$	$< 7.69\times10^{-2}$
Π_4	$gd\Delta\rho_{\max}/\overline{\rho}\Omega^2(b-a)^2$	$> 2.19\times10^{-2}$
Π_5	$4\Omega^2(b-a)^5/\overline{\nu}^2 d$	$< 1.91\times10^{8}$
Π_6	$\overline{\nu}/\overline{\kappa}$	7.21
Π_7	$\Delta T_{\max}/\overline{T}$	0.68×10^{-3}–0.16
Π_8	$\overline{c}\,\overline{T}/\Omega^2(b+a)^2$	$> 8.40\times10^{-2}$
B	$gd\sigma_z\Delta\rho_{\max}/4\Omega^2(b-a)^2\overline{\rho}$ (see equation (4.1))	$> 2\times10^{-3}$

fully developed baroclinic waves are fraught with mathematical difficulties which have not yet been fully overcome, even with the aid of large, high-speed electronic computers. Notwithstanding these mathematical difficulties in the theory of fully developed baroclinic waves, it was possible to show in connexion with the early wall-heated annulus experiments that the general form of the flow pattern could be accounted for in terms of a very simple theoretical model that treats

the 'jet-stream' associated with the waves as a quasi-geostrophic detached thermal boundary layer (see § 2 below). The model is upheld by the present experiments with systems subject to internal heating.

It was also shown in connexion with wall-heated systems (Rev.): (*a*) that Eady's inviscid theory of the baroclinic instability of flow characterized by uniform vertical shear and zero horizontal shear and by a linear vertical density gradient, when correctly applied, accounts remarkably well for the upper part of the anvil-shaped transition curve in a typical régime diagram with $\Pi_4 \equiv gd\Delta\rho_{\max}/\bar{\rho}\Omega^2(b-a)^2$ (a measure of the applied temperature contrast) as ordinate and $\Pi_5 \equiv 4\Omega^2(b-a)^5/\nu^2 d$ (an inverse measure of viscous friction) as abscissa (see figure 2 and table 2) when Π_5 exceeds about 10^7; (*b*) that certain attempts to explain the other parts of the transition curve—though valuable as extensions of Eady's original work to systems in which viscosity (and in one case the curvature of the side-walls) cannot be neglected—are inadequate because they account neither for the position of the 'knee' of the transition curve nor for the simple shape of the lower part of the curve; and (*c*) therefore that a successful theory will have to take into account, *inter alia*, viscous effects not only in end-wall boundary layers but also in side-wall boundary layers and in the main body of the fluid. These conclusions are upheld by the present experiments which indicate, among other things, that the upper transition is fairly insensitive to the details of the structure of the basic axisymmetric flow.

In what follows, the general theoretical ideas behind the experiments are discussed in § 2, the design and construction of apparatus are outlined in § 3 and the results of the experiments are presented in § 4.

2. Some theoretical ideas

(*a*) *Equations of the problem*

Consider a liquid of specific heat c, kinematic viscosity ν, thermal diffusivity κ and thermal coefficient of cubical expansion α, and assume for simplicity that c, ν, κ and α are constant. Also make use of the Boussinesq approximation, by which the density of the fluid is treated as uniform and equal to the mean density $\bar{\rho}$, but non-uniformity of the weight per unit volume, $|\boldsymbol{g}|(\bar{\rho}+\rho_1)$, is taken into account; here $\boldsymbol{g}$ is the acceleration of gravity and

$$\rho_1 = -\bar{\rho}\alpha(T-\bar{T}) \tag{2.1}$$

(see table 1). In addition, assume that (*a*) $|\boldsymbol{g}|$ is so much larger than centripetal acceleration that the latter can be ignored, and (*b*) effects due to variations of surface tension with temperature are negligible. These simplifications, though not *strictly* valid for the experiments (see Rev.), should suffice for the purpose of the present section.

The three components of the Navier–Stokes equations of hydrodynamical motion, Eulerian velocity $\boldsymbol{u} = (u, v, w)$ relative to a frame of reference which rotates with angular velocity $\boldsymbol{\Omega} = (0, 0, \Omega)$ relative to an inertial frame, and the equations of continuity and heat transfer are respectively as follows:

$$-2\Omega v + \frac{1}{\bar{\rho}}\frac{\partial p}{\partial r} = \nu\nabla^2 u - \left(u\frac{\partial u}{\partial r} + \frac{v}{r}\frac{\partial u}{\partial \phi} + w\frac{\partial u}{\partial z}\right) - \frac{\partial u}{\partial t} + \frac{v^2}{r}, \tag{2.2}$$

$$2\Omega u + \frac{1}{\bar{\rho}r}\frac{\partial p}{\partial \phi} = \nu\nabla^2 v - \left(u\frac{\partial v}{\partial r} + \frac{v}{r}\frac{\partial v}{\partial \phi} + w\frac{\partial v}{\partial z}\right) - \frac{\partial v}{\partial t} - \frac{uv}{r}, \tag{2.3}$$

$$-g\alpha(T-\bar{T}) + \frac{1}{\bar{\rho}}\frac{\partial p}{\partial z} = \nu\nabla^2 w - \left(u\frac{\partial w}{\partial r} + \frac{v}{r}\frac{\partial w}{\partial \phi} + w\frac{\partial w}{\partial z}\right) - \frac{\partial w}{\partial t}, \tag{2.4}$$

$$\frac{\partial u}{\partial r}+\frac{1}{r}\frac{\partial v}{\partial \phi}+\frac{\partial w}{\partial z}=-\frac{u}{r}, \tag{2.5}$$

$$\kappa\nabla^2 T+q-(\boldsymbol{u}.\nabla)\,T-\frac{\partial T}{\partial t}=0, \tag{2.6}$$

where (r,ϕ,z) are cylindrical polar coordinates (see table 1), p is the difference between the actual pressure and the hydrostatic pressure, $q\rho c$ is the rate (per unit volume) at which internal heat sources supply thermal energy to the liquid.

(b) *The impressed temperature field*

It is instructive to consider the form of the steady one-dimensional temperature field that would obtain after the system has been allowed to attain thermal equilibrium if the fluid were replaced by a solid with the same values of κ and q, assumed uniform and steady, when $(b-a)\ll\frac{1}{2}(b+a)$ so that $\kappa\nabla^2 T=\kappa\mathrm{d}^2T/\mathrm{d}r^2=-q$; then

$$T=(b-a)^{-1}[(r-a)\,T_b+(b-r)\,T_a]-q(r-a)\,(r-b)/2\kappa \tag{2.7}$$

where T_a and T_b are the temperatures of the cylindrical side-walls in $r=a$ and $r=b$ respectively. The (conductive) heat flow (in the r-direction) is given by

$$-\bar{\rho}c\kappa\frac{\mathrm{d}T}{\mathrm{d}r}=-\bar{\rho}c\kappa\left\{\frac{T_b-T_a}{b-a}-\frac{q}{\kappa}\,(r-\tfrac{1}{2}(a+b))\right\}. \tag{2.8}$$

The wall-heated case corresponds to $q=0$; then, by equations (2.7) and (2.8),

$$\text{(wall heating):}\quad T=\frac{(r-a)\,T_b+(b-r)\,T_a}{(b-a)},\quad \frac{\mathrm{d}T}{\mathrm{d}r}=\frac{T_b-T_a}{b-a}; \tag{2.9}$$

in this case the flux of heat is independent of r. On the other hand, the internally heated cases correspond to $q\neq 0$ and heat taken out of (but not put into) the fluid via the side-walls (i.e. $\mathrm{d}T/\mathrm{d}r\geqslant 0$ at $r=a$ and/or $\mathrm{d}T/\mathrm{d}r\leqslant 0$ at $r=b$). When all the heat is removed via the inner side-wall, $\mathrm{d}T/\mathrm{d}r=0$ at $r=b$ and

$$\text{(inner wall cooled):}\quad T=T_a+\frac{q}{2\kappa}\,(r-a)\,(2b-a-r),\quad \frac{\mathrm{d}T}{\mathrm{d}r}=\frac{q}{\kappa}\,(b-r); \tag{2.10}$$

when all the heat is removed via the outer side-wall, $\mathrm{d}T/\mathrm{d}r=0$ at $r=a$ and

$$\text{(outer wall cooled):}\quad T=T_a-\frac{q(r-a)^2}{2\kappa},\quad \frac{\mathrm{d}T}{\mathrm{d}r}=\frac{q}{\kappa}\,(a-r); \tag{2.11}$$

when the heat is removed at the same rate via both outer and inner side-walls simultaneously, $(\mathrm{d}T/\mathrm{d}r)_{r=a}=-(\mathrm{d}T/\mathrm{d}r)_{r=b}$ and

$$\text{(both walls cooled):}\quad T=T_a-\frac{q}{2\kappa}\,(r-a)\,(r-b),\quad \frac{\mathrm{d}T}{\mathrm{d}r}=-\frac{q}{\kappa}\,(r-\tfrac{1}{2}(b+a)). \tag{2.12}$$

The variation with r of T and $\mathrm{d}T/\mathrm{d}r$, as given by each of the foregoing expressions, is illustrated by the first and second columns of figure 3.

(c) *Geostrophy and the thermal wind equation*

When $\Omega=0$ convection in the system under consideration consists of rising motions in the warmer parts of the fluid, sinking motions in the cooler parts and no azimuthal flow (i.e. $v=0$ everywhere). As a result of gravitational torques individual fluid elements spin around horizontal axes as they circulate in meridian planes.

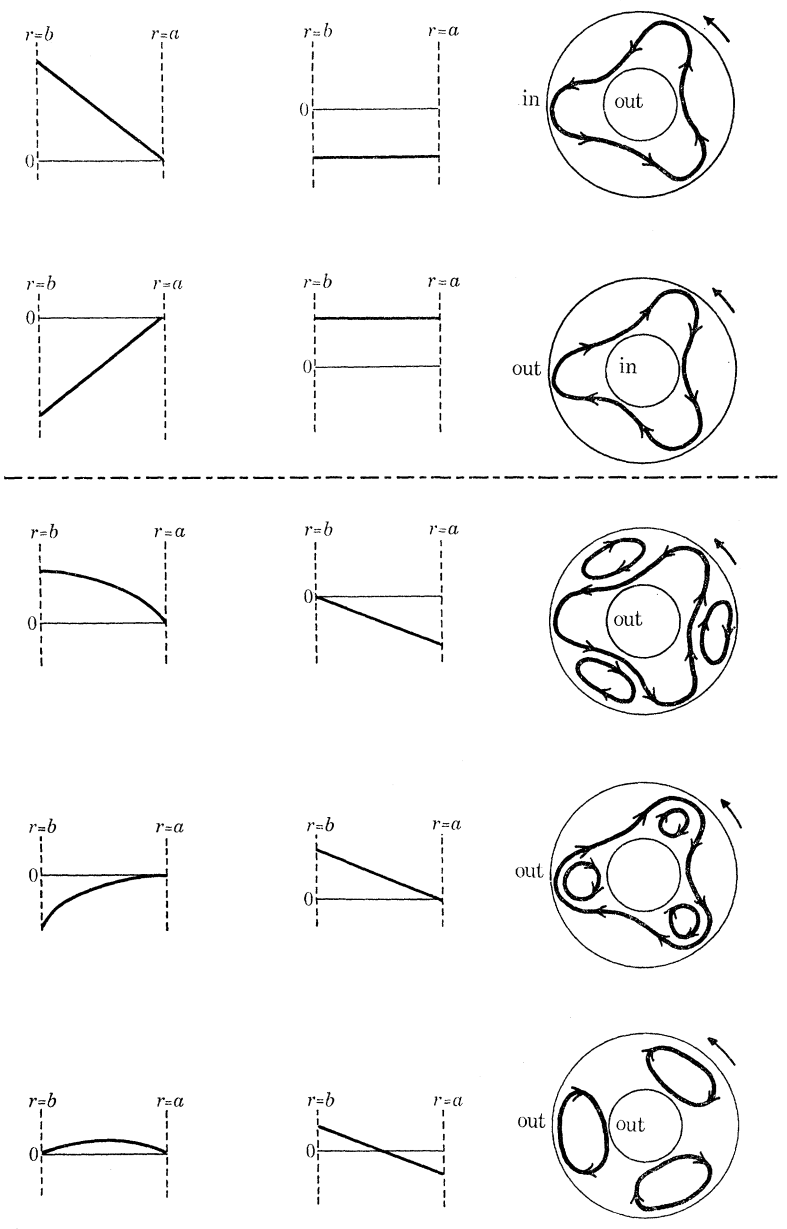

FIGURE 3. Schematic illustrations of the variations of the impressed temperature T with radius r (left column); $\mathrm{d}T/\mathrm{d}r$, proportional to minus the top-surface zonal velocity when the flow is axisymmetric (see equation (2.14)) (centre column); and the main characteristics of the top surface flow pattern in the steady waves régime according to predictions based on the integral constraints expressed by equation (2.19 *b*) (right column). (Basic rotation anticlockwise.) *First row*: outer wall heated and inner wall cooled. The top-surface flow is generally cyclonic (cf. first column of figure 5). *Second row*: inner wall heated and outer wall cooled. The top surface flow is generally anticyclonic (cf. second column of figure 5). *Third row*: internal heating, inner-wall cooled. As no heat crosses the outer wall (in $r = b$), equation (2.19 *b*) requires that $v_0(r \doteqdot b) = 0$ in the symmetrical régime and the presence of closed anticyclones in contact with the outer wall in the wave régime (cf. first row). *Fourth row*: internal heating, outer wall cooled. As no heat crosses the inner wall (in $r \doteqdot a$), equation (2.19 *b*) requires that $v_0\,(r \doteqdot a) = 0$ in the symmetrical régime and the presence of closed anticyclones in contact with the inner wall in the wave régime (cf. second row). *Fifth row*: internal heating, both walls cooled. Equation (2.19 *b*) requires that $v_0\,(r \doteqdot b) < 0$ and $v_0\,(r \doteqdot a) > 0$ in the symmetrical régime, and a wave-régime flow pattern consisting essentially of closed anticyclones in contact with both inner and outer walls. These predictions are borne out by the experiments illustrated in figures 5 to 9.

PHILOSOPHICAL TRANSACTIONS OF THE ROYAL SOCIETY A MATHEMATICAL, PHYSICAL & ENGINEERING SCIENCES

The action of very slow rotation produces weak azimuthal flow proportional to Ω, leaving the basic meridional circulation unaffected. However, the effect of very rapid rotation is quite different. Then, owing to the strong gyroscopic forces that oppose any tendency for individual fluid elements to spin about axes that are not parallel to $\mathbf{\Omega}$, a complete reorganization of the flow pattern must take place. Except within boundary layers of the Ekman type near $z = \pm \frac{1}{2}d$ and of more complex structure near $r = a$ and $r = b$, and possibly within detached shear layers in the main body of the fluid (see Rev.; also Hide 1967) the flow will be highly geostrophic, characterized by a balance between Coriolis forces and the non-hydrostatic component of the pressure gradient. Geostrophic motion, designated by the subscript '0', satisfies equations (2.2) to (2.4) when Ω is so large that all the 'ageostrophic' terms on the right-hand side of these equations tend to zero. Thus

$$\frac{1}{\bar{\rho}}\left(\frac{\partial p}{\partial r}, \frac{1}{r}\frac{\partial p}{\partial \phi}, \frac{\partial p}{\partial z}\right) = (-2\Omega v_0,\ 2\Omega u_0,\ g\alpha(T-\bar{T})). \tag{2.13}$$

Eliminate p between these equations and find the 'thermal wind equation'

$$2\Omega\left(\frac{\partial u_0}{\partial z}, \frac{\partial v_0}{\partial z}\right) = g\alpha\left(-\frac{1}{r}\frac{\partial T}{\partial \phi}, \frac{\partial T}{\partial r}\right) \tag{2.14}$$

relating the vertical shear of horizontal motion to the horizontal gradient of temperature.

The equations of geostrophy and the thermal wind equation are, of course, mathematically degenerate. They do not suffice when combined with appropriate boundary conditions to determine the field of flow completely; this can only be done by taking ageostrophic effects into account. Nevertheless, these equations express with good accuracy important properties that slow hydrodynamical motions in rapidly rotating systems must possess nearly everywhere and, as we shall show in what follows next (see also Hide 1958), when combined with considerations of heat transfer at the bounding surfaces of the system, they lead to useful expressions for certain integral properties that the top-surface flow pattern must possess.

(*d*) *Horizontal heat transfer and the top-surface flow pattern*

Define the quantity $H = H(r, \phi, t)$ as follows:

$$H \equiv \int_{-\frac{1}{2}d}^{\frac{1}{2}d}\left[-\kappa\frac{\partial T}{\partial r} + u(T-\bar{T})\right]\mathrm{d}z; \tag{2.15}$$

$\bar{\rho}crH\,\mathrm{d}\phi$ is the rate at which heat is transferred in the r direction across an imaginary vertical strip whose corners are located in $(r, \phi \pm \frac{1}{2}d\phi, \pm\frac{1}{2}d)$.

Axisymmetric flow

Because $u_0 = (2\Omega\bar{\rho}r)^{-1}\,\partial p/\partial\phi$, when the flow is axisymmetric the geostrophic part of $\boldsymbol{u}$ is purely azimuthal at all r and therefore makes no contribution to H. The only contribution to the second term on the right-hand side of equation (2.15) is due to ageostrophic flows in Ekman boundary layers near $z = \pm\frac{1}{2}d$ and possibly in detached shear layers at other values of z. Thus, it may be shown that (see Hide 1967)

$$H(r,t) \doteqdot -\int_{-\frac{1}{2}d}^{\frac{1}{2}d}\kappa\frac{\partial T}{\partial r}\,\mathrm{d}z - \frac{1}{2}\left(\frac{\nu}{\Omega}\right)^{\frac{1}{2}}\{Sv_0(r, \tfrac{1}{2}d, t)\,[T(r, \tfrac{1}{2}d, t) - \bar{T}] + v_0(r, -\tfrac{1}{2}d, t)\,[T(r, -\tfrac{1}{2}d, t) - \bar{T}]\}. \tag{2.16}$$

The dimensionless quantity S is introduced so that equation (2.16) applies to the case when the upper surface is free as well as when the upper surface is in contact with a rigid lid. Thus, S is defined as the ratio of the radial ageostrophic mass flux in the upper part of the fluid, above the Ekman layer in $z = -\frac{1}{2}d$, to that which occurs (in the opposite direction) in the Ekman layer near $z = -\frac{1}{2}d$ when the upper surface is in contact with a rigid lid, in which case $S \equiv 1$. The relative insensitivity of the measured heat flow to the upper surface boundary condition (see Rev.; also § 4 below) shows that S is also close to unity when the upper surface is free, implying the existence of an ageostrophic detached shear layer in the main body of the fluid.

Now, outside thin thermal boundary layers on the side-walls in $r = a$ and $r = b$ the contribution of thermal conduction to $H(r,t)$ is typically much less than the advective term and can be neglected in this approximate theory. If we make the reasonable assumptions that

$$T(r, \tfrac{1}{2}d, t) - \overline{T} \doteqdot \overline{T} - T(r, -\tfrac{1}{2}d, t) \doteqdot \tfrac{1}{2}[T(r, \tfrac{1}{2}d, t) - T(r, -\tfrac{1}{2}d, t)]$$

and $S \doteqdot 1$ then equation (2.16) becomes

$$H(r,t) \doteqdot -\frac{1}{4}\left(\frac{\nu}{\Omega}\right)^{\frac{1}{2}}[T(r, \tfrac{1}{2}d, t) - T(r, -\tfrac{1}{2}d, t)][v_0(r, \tfrac{1}{2}d, t) - v_0(r, -\tfrac{1}{2}d, t)]. \tag{2.17a}$$

The quantity $[T(r, \frac{1}{2}d, t) - T(r, -\frac{1}{2}d, t)]$ must be positive (or zero) for a fluid with a positive volume coefficient of thermal expansion, since otherwise the concomitant density distribution would be top-heavy and overturn. Therefore the first term in square brackets on the right-hand side of the last equation must be positive (or zero). As for the other term, this must equal $v_0(r, \frac{1}{2}d, t)$ multiplied by 2 when the upper surface is in contact with a rigid lid (for then, by symmetry, $v_0(r, \frac{1}{2}d, t) = -v_0(r, -\frac{1}{2}d, t)$) and by approximately 1 when the upper surface is free (for then $|v_0(r, -\frac{1}{2}d, t)| \ll |v_0(r, \frac{1}{2}d, t)|$). Hence

$$H(r,t) = (\text{negative definite quantity}) \times v_0(r, \tfrac{1}{2}d, t). \tag{2.17b}$$

Non-axisymmetric flow

When the pressure field is non-axisymmetric (as in the case of baroclinic waves) the geostrophic part of $\boldsymbol{u}$ is no longer entirely azimuthal at all r and equations (2.16) and (2.17) do not in general apply. However, for any cylindrical surface $r = r^*$ over which $|u_0|$ is everywhere much less than $|v_0|$ expressions comparable to equations (2.16) and (2.17) can be obtained using similar arguments. Thus, if we introduce the quantities $\mathscr{H}(r^*,t)$, $\Gamma(r^*,z,t)$ and $\hat{T}(r^*,z,t)$ defined as follows:

$$\mathscr{H}(r^*,t) \equiv \oint_0^{2\pi} H(r^*,\phi,t)\, r\,\mathrm{d}\phi, \tag{2.18a}$$

$$\Gamma(r^*,z,t) \equiv \oint_0^{2\pi} v_0(r^*,\phi,z,t)\, r\,\mathrm{d}\phi, \tag{2.18b}$$

and

$$\hat{T}(r^*,z,t) \equiv \frac{1}{2\pi}\oint_0^{2\pi} T(r^*,\phi,z,t)\, d\phi \tag{2.18c}$$

(where H, v_0 and T now depend on ϕ as well as on r, z and t), then in place of equations (2.17) we have

$$\mathscr{H}(r^*,t) \doteqdot -\frac{1}{4}\left(\frac{\nu}{\Omega}\right)^{\frac{1}{2}}[\hat{T}(r^*, \tfrac{1}{2}d, t) - \hat{T}(r^*, -\tfrac{1}{2}d, t)][\Gamma(r^*, \tfrac{1}{2}d, t) - \Gamma(r^*, -\tfrac{1}{2}d, t)] \tag{2.19a}$$

and

$$\mathscr{H}(r^*,t) = (\text{negative definite quantity}) \times \Gamma(r^*, \tfrac{1}{2}d, t). \tag{2.19b}$$

Except in very special circumstances we expect to find two values of r^*, one a little greater than a and the other a little less than b.

Equation (2.17 a) and one equivalent to equation (2.19 b) were deduced by Hide (1967, 1958) and successfully used in the interpretation of experimental determinations of heat transfer by axisymmetric flow and of the general form of non-axisymmetric flow patterns observed in wall-heated systems. We shall conclude the present section with a discussion of the implications of equations (2.17) and (2.19) concerning the general form of the top-surface flow patterns expected in systems subject to internal heating.

(*e*) *Some predictions*

First consider cases of axisymmetric flow. According to equation (2.14) the horizontal profile of zonal geostrophic velocity, $v_0(r)$, is *qualitatively* the same as that of $\mathrm{d}T/\mathrm{d}r$ (see middle column of figure 3). As v_0 only vanishes at those values of r across which no heat transfer takes place, it has this property at one value of r in each of the internally heated systems (see figure 3). Note the principal characteristics of the profiles $v_0(r)$ in the separate cases illustrated. At the 'thermal equator', where $H = 0$, by equations (2.17) $v_0 = 0$.

When the flow is non-axisymmetric we can apply equations (2.19) to the surfaces $r \doteqdot a$ and $r \doteqdot b$. The wall-heated cases (see figures 3 a, b and equation (2.9)) have been discussed elsewhere (Hide 1958), where it is shown that patterns of the form illustrated—characterized by $\Gamma(r \doteqdot b) > 0$ and $\Gamma(r \doteqdot a) > 0$ (see equation (2.18)) when $T_b > T_a$ and by $\Gamma(r \doteqdot b) < 0$ and $\Gamma(r \doteqdot a) < 0$ when $T_b < T_a$—are consistent with the constraints of geostrophy as expressed here by equation (2.19 b).

According to that equation, $\Gamma(r \doteqdot b) = 0$ when no heat crosses the outer side-wall. Figure 3 c illustrates how the pattern of figure 3 a can be modified in order to meet this new requirement. The essential modification is the addition of strong anticyclonic eddies in which the easterly flow near $r = b$ is sufficient to annul the contribution of the main westerly jet to $\Gamma(r \doteqdot b)$. Likewise, $\Gamma(r \doteqdot a) = 0$ when no heat crosses the inner side-wall and figure 3 d illustrates how the pattern of figure 3 b must be modified, in this case by adding anticyclonic eddies in which the westerly flow near $r = a$ is sufficient to annul the contribution of the main easterly jet to $\Gamma(r \doteqdot a)$. But possibly the most interesting case of all is that illustrated by figure 3 e. Then, in contrast to wall-heated systems, $\Gamma(r \doteqdot a)$ and $\Gamma(r \doteqdot b)$ must be of opposite sign, and this requires that the main horizontal circulation consist of anticyclones extending from $r = a$ to $r = b$. These predictions accord well with the experiments described below.

3. Apparatus

The ranges of experimental conditions covered by the investigation are summarized in table 3. The apparatus used was similar in many of its general features to that used in the original annulus experiments. Many of the details of design and construction are as described in earlier papers (see Rev.) and in what follows we restrict attention to essential and novel features.

(*a*) *Convection chamber*

The convection chamber (see figure 1) is the annular space of height 16 cm between two copper cylinders, the outer one with inner radius $b = 8.55$ cm and the inner one with outer radius $a = 5.71$, 4.06 or 0.04 cm. The cylinders were secured to an electrically insulating base-plate

mounted on a horizontal turntable. The effective bottom of the convection chamber, located in $z = -\frac{1}{2}d$ and shown schematically in figure 1, was the upper surface of a Perspex annular ring which projected above the level of the floors of the water baths.

TABLE 3. VALUES OF EXPERIMENTAL PARAMETERS

parameter	value or approximate range
a/cm	4.06, 5.06 (see note 1), 5.71, 0.04 (see note 2)
b/cm	8.55
$(b-a)$/cm	2.84, 3.49 (see note 1), 4.49, 8.51 (see note 2)
d/cm	6, 12
Ω/rad s^{-1}	0–4
$\lvert T_b - T_a\rvert$/K	0.2–30
$(T_{\sqrt{(ab)}} - T_a)$/K	0.2–30 (see note 3)
$\Delta T_{\max}$/K	0.2–40
$\sigma_z \Delta T_{\max}$/K	0.2–30
P/J s^{-1}	1–500
$\lvert\rho(T_b) - \rho(T_a)\rvert$ or $\rho(T_{\sqrt{(ab)}}) - \rho(T_a)$/g cm^{-3}	$(0.04\text{–}10.00) \times 10^{-3}$
$\Delta\rho_{\max}$/g cm^{-3}	$(0.05\text{–}13.00) \times 10^{-3}$
$\bar{\nu}$/cm^2 s^{-1} (see note 4)	1.01×10^{-2}
$\bar{\kappa}$/J cm^{-1} s^{-1} K^{-1}	5.86×10^{-3}
$\bar{c}$/J g^{-1} K^{-1}	4.184
$\bar{\chi}$/cm^2 s^{-1}	1.41×10^{-3}
$\bar{\rho}$/g cm^{-3}	0.998

Note 1: Perspex inner cylinder; note 2: fine wire as inner cylinder; note 3: see equation (3.7); note 4: the liquid used in all the experiments described in this paper was effectively water so far as $\bar{\nu}, \bar{\kappa}, \bar{c}, \bar{\rho}$ etc. were concerned, but contained traces of potassium sulphate and detergent which rendered the liquid electrically conducting (cf. figure 1).

The top of the convection chamber carried a fixed Perspex lid, placed in contact with the upper surface of the liquid in the convection chamber (in $z = \frac{1}{2}d = 6.0$ or 3.0 cm) in some of the experiments, but kept in place in order to eliminate effects due to evaporation and 'wind stress' when, as in most of the experiments, the upper surface was free.

The two gap-widths $(b-a)$ used in most of the experiments were 4.49 and 2.84 cm (corresponding to $a = 5.71$ or 4.06 cm) and did not, as a result of slight unavoidable eccentricities in shape of the bounding cylindrical side-walls of the convection chamber, deviate from these values by more than $\pm 1\,\%$. Errors in the vertical alinement of the side-walls and the horizontal alinement of the base amounted to $\pm 5 \times 10^{-4}$ rad. The depth d was measured to an accuracy of 0.05 cm by means of a dipstick.

(*b*) *Turntable*

The turntable was driven by a synchronous induction motor via a Graham continuously variable speed transmission unit. Typical values of Ω were 0 to 4 rad s^{-1} and could be maintained constant to an accuracy of 0.1 % over periods of the order of 0.5 h and to 0.5 % over several hours. Individual rotation periods, $2\pi/\Omega$, could be measured by means of an electronic timing unit actuated when a beam of light from a lamp fixed in the laboratory was reflected by a plane mirror mounted on the turntable on to a photocell fixed in the laboratory.

(*c*) *Temperature control and internal heating*

The temperature baths in contact with the copper side-walls (see figure 1) could be supplied individually with water circulating at about 50 cm^3 s^{-1} and kept at constant temperature (to within ± 0.05 K) by means of thermostats.

PHILOSOPHICAL TRANSACTIONS OF THE ROYAL SOCIETY A MATHEMATICAL, PHYSICAL & ENGINEERING SCIENCES

When only one wall was cooled the part played by the warm copper wall was uncertain. However, one experiment, involving the replacement of the warm copper cylinder with a Perspex cylinder carrying an electrode (comprising a spiral of 8 turns of 0.8 cm diameter copper wire in a groove), indicated that the flow is not in most circumstances sensitive to the thermal properties of the warm wall.

Internal heating was achieved by passing an a.c. electric current through the liquid in the convection chamber. This liquid was a weak aqueous solution of potassium sulphate (plus a trace of detergent which reduced surface tension effects) with electrical resistance of 100–200 Ω. The electrical power supply was connected to the convection chamber via high-quality silver-graphite slip rings of electrical resistance about 10^{-3} of that of the liquid in the convection chamber. The voltage of the 50 Hz a.c. power supply could be varied from 0 to 300 V by means of a variable auto-transformer. The copper cylinders themselves were the electrodes across which this voltage was applied. As the electrode resistance was only 1 mΩ, azimuthal and vertical variations in current density were negligible. Owing to the geometry of the system, the current density varied as r^{-1}; the corresponding radial dependence of q (the internal heating rate per unit volume divided by $\bar{\sigma}\bar{\rho}$) was r^{-2} times a slowly varying factor associated with the variation of electrical conductivity with temperature.

The tendency for electrical conductivity to increase with temperature (by nearly 2 % K^{-1}) was a complicating factor whose possible effects, though not serious in the experiments, have not been fully investigated. One effect should be an increase in the vertical stability, since q will be higher in the warm upper regions than in the cooler lower regions.

Voltage and current were measured by means of suitably calibrated dial instruments to an accuracy of ± 1 % each, giving an overall error of ± 2 % in P, the electrical power input. By definition

$$P \equiv \int_a^b \int_{-\frac{1}{2}d}^{\frac{1}{2}d} \int_0^{2\pi} 2\pi q(r)\, r\, \mathrm{d}\phi\, \mathrm{d}z\, \mathrm{d}r \tag{3.1}$$

(see equation (2.6)), typical values of which were 1 to 500 J s^{-1}. P could be maintained constant to better than 2 % throughout each experiment.

(*d*) *Temperature measurements*

The quantity $T_b - T_a$ was taken as the average of the readings of three copper/constantan thermocouples mounted at different levels, each recording the temperature difference between a point on the outer wall of the outer cylinder and the inner wall of the inner cylinder. Each thermojunction was held in place by a thick layer of epoxy resin, which thermally insulated the junction from the water bath but held it in close contact with the cylinder, from which it was electrically insulated by a thin layer of epoxy resin. Because the cylinders were made of copper, temperature gradients within them were small. The estimated error of measurement of $T_b - T_a$ ranged from ± 3 % at $|T_b - T_a| \geqslant 3$ K to ± 25 % at $|T_b - T_a| \doteqdot 0.2$ K and was due largely to very slight fluctuations in temperature of the thermostatically controlled temperature baths.

Figure 4 shows the positions of thermojunctions mounted in an array placed within the fluid, all at the same value of the azimuthal angle, namely $\phi = 0$.

The thermocouples thus formed by the thermojunctions were made from 5×10^{-3} in (1.26×10^{-2} cm) diameter copper and constantan wire. They were shielded from the electrical effects of the heating current by layers of lacquer and silicone grease insulation. The electrical signals from the thermocouples were led to d.c. amplifiers and chart recorders via low-noise silver-graphite slip rings. Calibration was effected by means of a high-quality potentiometer.

Hide (1967) has introduced a quantity σ_z where, in the case of wall heating,

$$\sigma_z \equiv |T_b - T_a|^{-1} \int_a^b \int_{-\frac{1}{2}d}^{\frac{1}{2}d} \int_0^{2\pi} r \frac{\partial T}{\partial z} \, \mathrm{d}\phi \, \mathrm{d}z \, \mathrm{d}r \Big/ \pi(b^2 - a^2). \tag{3.2}$$

$\sigma_z |T_b - T_a|/d$ is the mean vertical temperature gradient set up by the fluid motion itself (see § 4 below). In order to extend this definition of σ_z to the case of internal heating, we must replace $|T_b - T_a|$ by $\Delta T_{\max}$, the difference in temperature between the warmest and the coolest points in the convecting fluid.

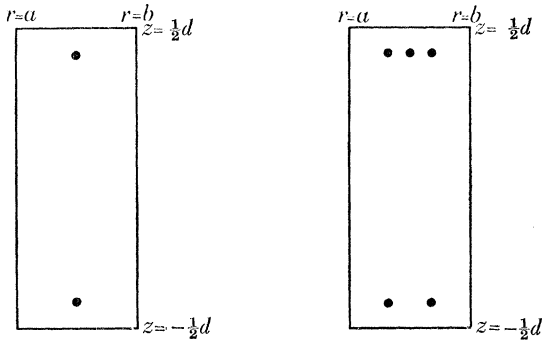

(a) (b)

FIGURE 4. Illustrating the positions (r, ϕ, z) within the convection chamber of the points at which temperature measurements were made by means of thermocouples

(a) $(\frac{1}{2}(a+b), 0, \frac{5}{12}d)$, $(\frac{1}{2}(a+b), 0, -\frac{5}{12}d)$

(b) $((2a+b)/3, 0, \frac{5}{12}d)$, $(\frac{1}{2}(a+b), 0, \frac{5}{12}d)$, $((2b+a)/3, 0, \frac{5}{12}d)$, $((2a+b)/3, 0, -\frac{5}{12}d)$ and $((2b+a)/3, 0, -\frac{5}{12}d)$.

Estimates of $\Delta T_{\max}$ and of the mean vertical temperature contrast $(\sigma_z \Delta T_{\max})$ were deduced from readings of the thermocouples in the array (see figure 4) and on the side-walls, linear extrapolation and interpolation and the following expressions for $T'(a \text{ or } b, z)$ defined as the mean with respect to ϕ of the temperature just outside the thermal boundary layer on the side-wall in $r = a$ or $r = b$ being used:

$$\begin{aligned}
&\text{outer wall cooled:} \quad T'(a, 0) \doteq T_a, \quad T'(b, -\tfrac{1}{2}d) \doteq T_b;\\
&\text{inner wall cooled:} \quad T'(b, 0) \doteq T_b, \quad T'(a, -\tfrac{1}{2}d) \doteq T_a;\\
&\text{both walls cooled:} \quad T'(b, -\tfrac{1}{2}d) \doteq T_b, \quad T'(a, -\tfrac{1}{2}d) \doteq T_a,\\
&\qquad\qquad T_{\sqrt{(ab)}} \doteq \overline{T(\tfrac{1}{2}(a+b), \phi, 0)};
\end{aligned}$$

here $T_{\sqrt{(ab)}}$ is defined by equation (3.7) below and the bar denotes 'average with respect to ϕ over the range 0 to 2π'. These relations follow from considerations of the heat flow by conduction across the thermal boundary layers on the side-walls. Thus, as the net heat transfer must be zero for a side-wall through which no heat is being extracted, it is plausible to assume that the average with respect to ϕ of the temperature contrast across the boundary layer must be zero near $z = 0$. Similar arguments applied to a side-wall through which heat *is* being extracted indicate that the corresponding temperature contrast then vanishes lower down, near $z = -\frac{1}{2}d$. When estimating σ_z for the wall-heating case from thermocouple-array measurements, account was

taken of the z-dependence of $\partial T/\partial z$ by assuming that $\partial T/\partial z$ at $|z| > \frac{5}{12}d$ is 0.5 times its value when $|z| < \frac{5}{12}d$ (see Hide 1958, 1970; Kaiser 1969).

(*e*) *Heat flow measurements*

A convenient dimensionless measure of heat flow is the Nusselt number, N, although difficulties arise in defining N when internal heat sources are present. As all heat leaves the system by conduction across bounding surfaces we can define N as follows:

$$N \equiv \left[\int\int_{\text{out}} \nabla T . \mathrm{d}\boldsymbol{s}\right] \Big/ \left[\int\int_{\text{out}} (\nabla T)_{\text{cond.}} . \mathrm{d}\boldsymbol{s}\right]. \tag{3.3}$$

Here the numerator is proportional to the total steady heat flow through the convecting system if the integral is taken over those parts of the bounding surfaces where heat leaves the system, $\mathrm{d}\boldsymbol{s}$ being an element of area of those surfaces. The denominator is the corresponding integral for what we shall here term 'the corresponding conductive system'.

In the case of wall-heating (see figures 3 *a*, *b*) the 'corresponding conductive system' is readily defined; one simply replaces the fluid by a solid with the same thermal conductivity, keeping the thermal properties of the bounding surfaces the same as in the convecting case. Then (see Hide 1958)

$$N = \frac{(\text{total rate of heat transfer}) \ln (b/a)}{2\pi |T_b - T_a| \, \mathrm{d}\kappa\bar{\rho}\bar{c}}. \tag{3.4}$$

In the case of internal heating with one side-wall cooled and the other (effectively) an insulator (see figures 3 *c*, *d*), the 'corresponding conductive system' is that in which (i) the fluid is replaced by a solid of the same thermal conductivity, (ii) the temperature of the bounding cylinders are T_a and T_b and $\partial T/\partial r = 0$ over the 'insulating' side-wall (namely $r = b$ in figure 3 *c* and $r = a$ in figure 3 *d*), and (iii) the hypothetical internal heat supply has the same radial dependence ($q \propto r^{-2}$, see above) as in the convective case but not, of course, the same magnitude. Integrating equation (2.6) when $T = T(r)$, $\boldsymbol{u} = \partial T/\partial t = 0$, we find:

$$N = \frac{P \ln (b/a)}{4\pi |T_b - T_a| \, d\kappa\bar{\rho}\bar{c}} \quad \text{(inner or outer wall cooled)} \tag{3.5}$$

(cf. figures 3 *c*, *d* and equation (3.1)), and

$$N = \frac{P \ln (b/a)}{16\pi (T_{\sqrt{(ab)}} - T_a) \, d\kappa\bar{\rho}\bar{c}} \quad \text{(both walls cooled)} \tag{3.6}$$

(cf. figure 3 *e*). Here

$$T_{\sqrt{(ab)}} \equiv \frac{1}{2\pi d} \int_0^{2\pi} \int_{-\frac{1}{2}d}^{\frac{1}{2}d} T(\sqrt{(ab)}, \phi, z) \, \mathrm{d}z \, \mathrm{d}\phi \tag{3.7}$$

($r = \sqrt{(ab)}$ being the value of r at which $\mathrm{d}T/\mathrm{d}r$ vanishes in the 'corresponding conductive system'), T_a, the mean temperature of the inner wall, being held in this case at the same value as T_b, the temperature of the outer wall. Observe that one property of an annular system with $q \propto r^{-2}$ is that if the conduction of heat out of the system is apportioned equally between the two side-walls then $T_a = T_b$.

Determinations of N were made to an estimated accuracy of about $\pm 10\,\%$ (see § 4 below). Greater accuracy (*ca.* $\pm 1\,\%$) can be attained with apparatus specially designed for heat flow work (see Rev.), in which all spurious heat exchange effects are eliminated, but not with apparatus designed for visual studies, as in the experiments described below.

(*f*) *Flow visualization*

Most observations were made on clean aluminium particles either in suspension in large numbers in the main body of the fluid or in smaller numbers on the top surface. The latter method, especially when combined with streak photography, was best for studying regular flow patterns, while the former was most suitable for: (i) irregular flow patterns (see Rev.) when the upper surface was free, and (ii) all flow patterns when the upper surface was in contact with a rigid lid. Figures 6 and 7 illustrate (among other things) the use of these two methods on essentially similar flow patterns.

(*g*) *Experimental procedure*

The procedure for making each experimental run consisted of: (i) setting the angular speed of the turntable, the power input and the temperature(s) of the cooling bath(s) at predetermined values, (ii) waiting until it seemed, from the readings of thermocouples immersed in the fluid, that transient phenomena associated with the setting-up process had disappeared, (iii) waiting a further interval of time about twice the previous interval (amounting altogether to 1 or 2 h when $\Delta T_{\max} \simeq 30$ K, 10 K or 3 K and as much as 7 h when $\Delta T_{\max} \simeq 0.2$ K (see table 3)), and (iv) then carrying out the various measurements required.

4. Experimental results

The first part of the investigation demonstrated that the principal types of flow arising in systems subject to internal heating are the same as those found previously in the wall-heated case (see figures 5 to 12). The remainder of the investigation was concerned with the experimental determination of various properties of the velocity and temperature fields (see figures 5 to 14 and 17), heat flow (see figure 16) and the transition between axisymmetric and non-axisymmetric types of flow (see figure 15) and with the theoretical interpretation of the experimental results. In what follows it will be convenient to discuss axisymmetric flows, steady waves and vacillating and irregular flows under three separate headings.

(*a*) *Axisymmetric flow*

Streak photographs of the top-surface flow, each taken with a 1 s exposure, are given in figures 5 to 12. Examples of axisymmetric flows are given in figures 5 *a*, *d* (wall-heating), figures 6 *a*, *b*, *c* (respectively internal heating cases with the inner-wall cooled, outer-wall cooled and both walls cooled simultaneously), figures 8 *a*, *b*, *c* (the counterparts of figures 6 *a*, *b*, *c* when the gap-width $b-a$ is 2.84 cm instead of 4.49 cm) and figure 12 *a* (the case of an open cylinder with internal heating and the outer-wall cooled).

Top-surface azimuthal velocity profiles based on figures 6 *a*, *b*, *c* and 8 *a*, *b*, *c* are given in figure 13. Viscous boundary layers, required in general in order to satisfy the no-slip condition $v = 0$ on $r = a$ and $r = b$, are absent on $r = b$ in figures 13 *a*, *d* and on $r = a$ in figures 13 *b*, *e*, and v reverses sign at a certain value of r in figures 13 *c*, *f*. These results are in agreement with equations (2.17), according to which the geostrophic value of the azimuthal component of velocity, v_0, is proportional to the radial heat flow, $\mathscr{H}(r)$.

Equations (2.17) are only strictly valid in the geostrophic limit, when in magnitude $v/r\Omega$, a Rossby number, is typically much less than unity. The *maximum* Rossby numbers for figures

13 a to f are approximately 0.87, 0.49, 0.28, 0.25, 0.14 and 0.15 respectively. These quantities are rough measures of the errors expected from the application of equations (2.17) to (2.19).

In going from equation (2.16) to equations (2.17) it was assumed that the quantity S (a dimensionless measure of the ageostrophic flow in the upper part of the fluid when the top surface is

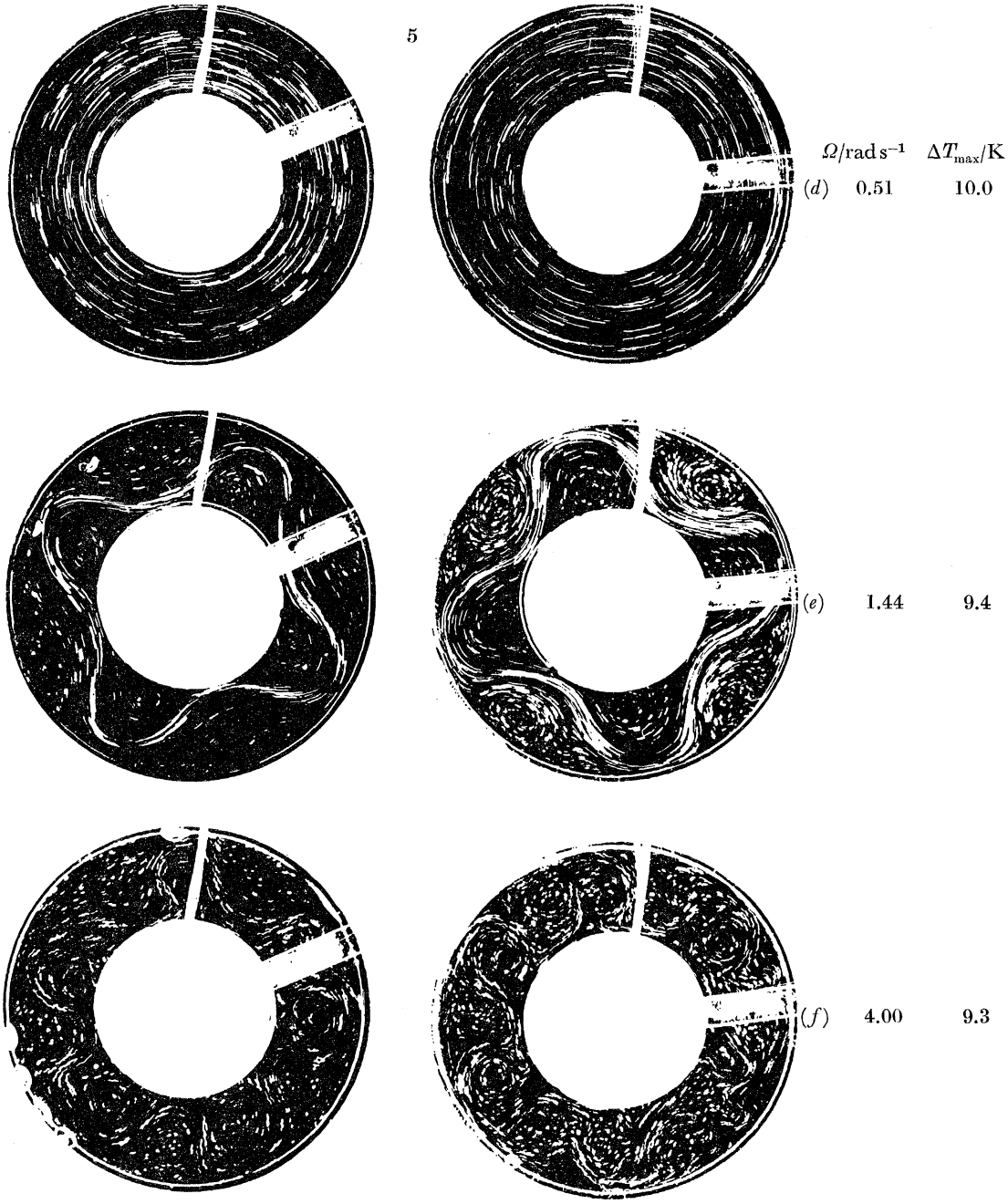

FIGURE 5. Streak photographs illustrating top surface flow patterns in two wall-heated cases, namely inner wall cooled (left column) and outer wall cooled (right column). The first row gives examples of the axisymmetric flow that occurs at sufficiently high values of $|T_b - T_a|$ and low values of Ω (cf. tables 1 and 2 and figure 2). The second row are typical examples of the steady baroclinic waves characteristic of moderate values of Ω, and the third row are typical examples of the unsteady baroclinic waves found at the largest values of Ω used in the experiments. (Liquid used: water, upper surface: free; basic rotation: anticlockwise; $a = 4.06$ cm, $b = 8.55$ cm, $d = 12.0$ cm.)

free) is close to unity. On substituting measured values of v_0, $\mathscr{H}$ (based on P (see equation (3.1))) and the vertical temperature contrast at $r = \frac{1}{2}(a+b)$ (see § 3), we find that for the cases corresponding to figures 13 *a*, *b*, *d*, *e* the respective values of S are 1.0, 0.7, 1.0 and 1.4. (Lack of internal temperature measurements at appropriate values of r precludes the calculation of S for figures 13 *c*, *f*.)

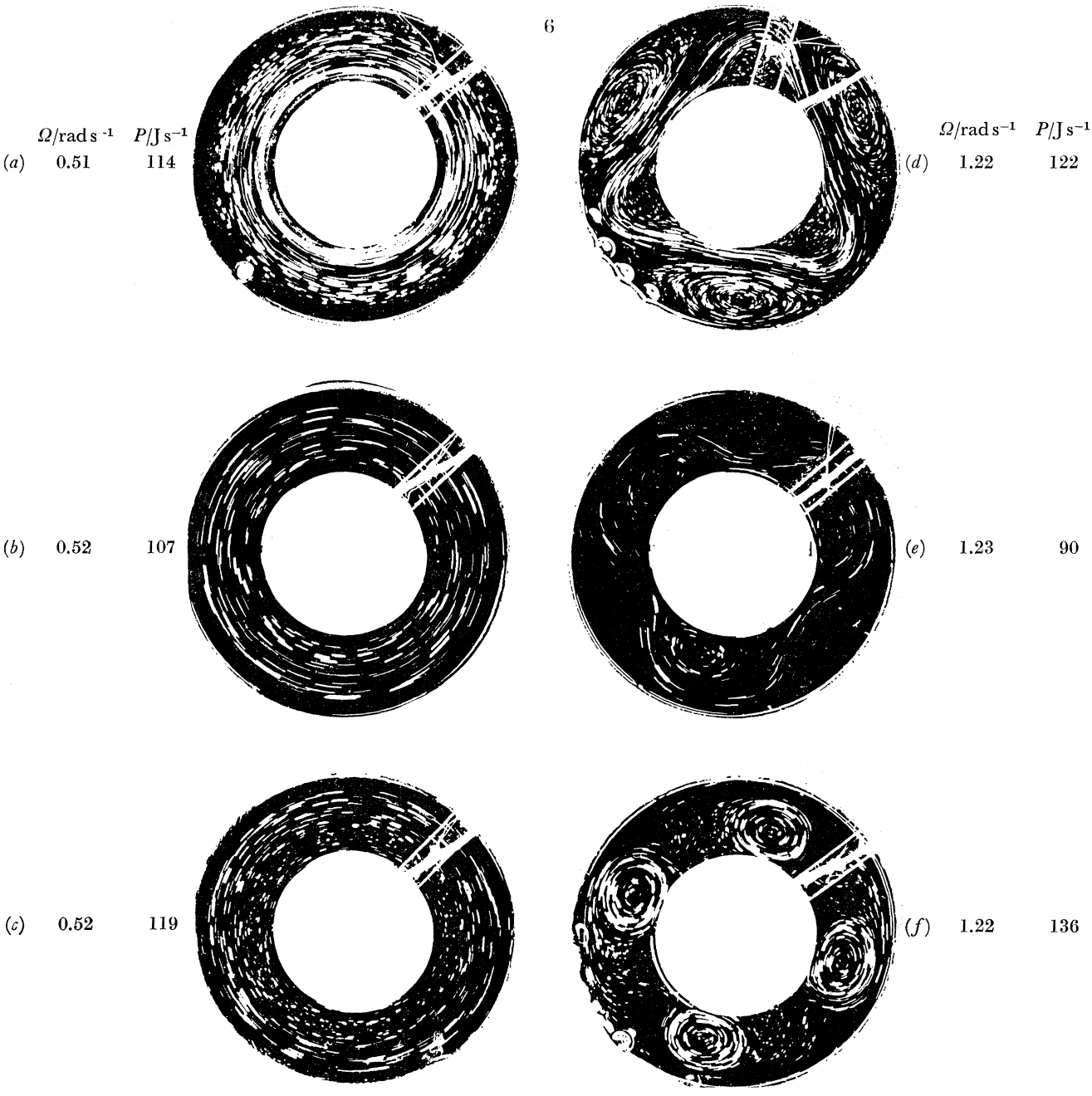

FIGURE 6. Streak photographs illustrating the top surface flow patterns in the symmetric régime (left column) and the steady waves régime (right column) of thermal convection in an internally heated rotating fluid annulus. The pictures illustrate the dependence of the general characteristics of the flow pattern on the manner by which heat is removed from the system (top row, inner wall cooled; middle row, outer wall cooled; bottom row, both walls cooled) and confirm the theoretical predictions of § 2, as illustrated by figure 3. (Liquid used: water; upper surface: free; basic rotation: anticlockwise; $a = 4.06$ cm, $b = 8.55$ cm, $d = 12.0$ cm.)

Figures 16 illustrate the dependence on Ω of the dimensionless heat flow parameter N (see equations (3.3) to (3.6)). As in the case of wall heating, within the axisymmetric régime N decreases with increasing Ω, as would be expected on theoretical grounds (see Hide 1967).

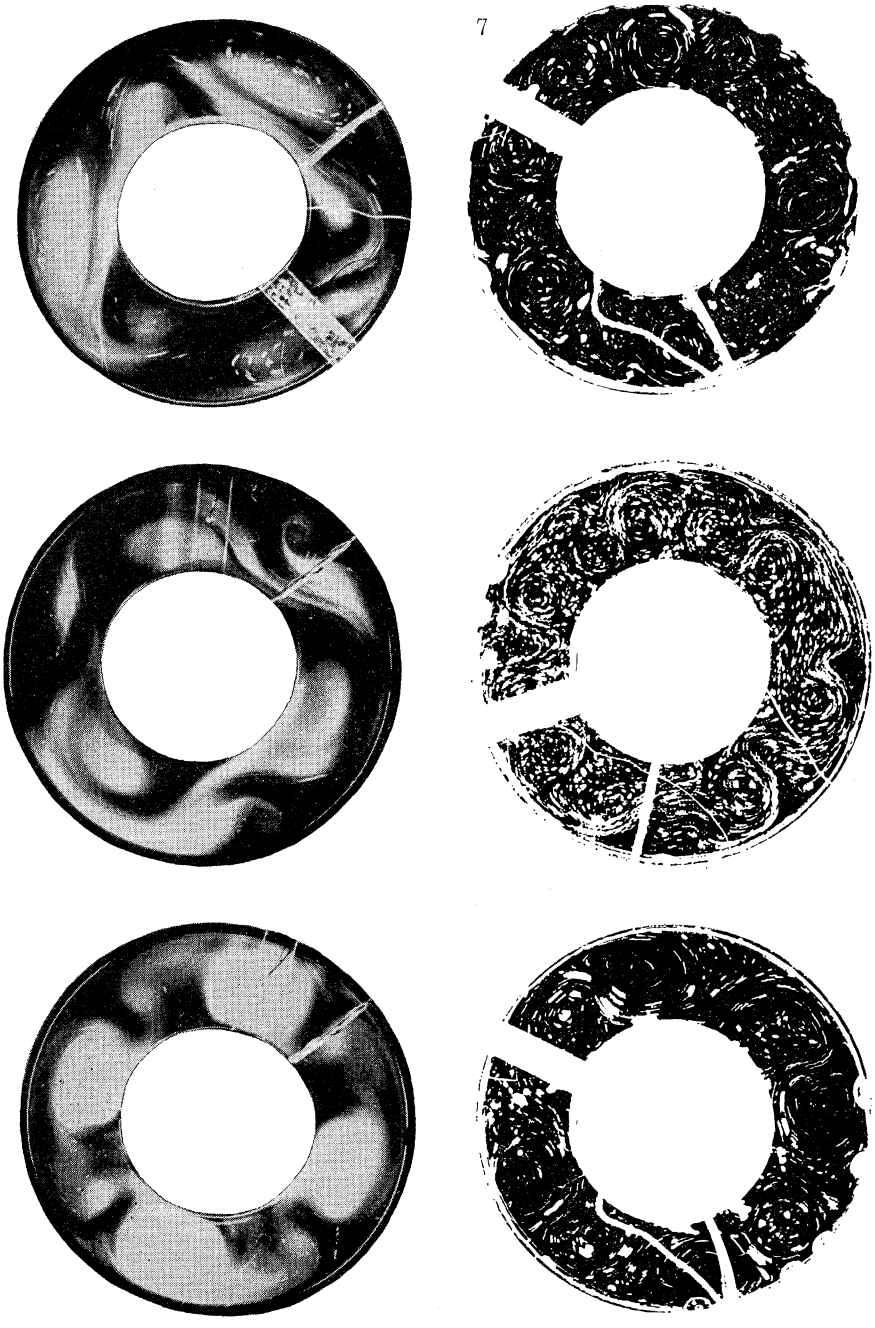

FIGURE 7. Further photographs illustrating top-surface flow patterns in an internally heated rotating fluid annulus. The first column shows the appearance of the steady-wave flows illustrated by the second column of figure 6 when aluminium powder in suspension is used as the flow-visualization technique. The second column consists of streak photographs of the irregular waves that occur at somewhat larger values of Ω. Top row, inner wall cooled; middle row, outer wall cooled; bottom row, both walls cooled. (Liquid used: water; upper surface: free; basic rotation: anticlockwise; $a = 4.06$ cm, $b = 8.55$ cm, $d = 12.0$ cm.)

Vertical temperature contrast and baroclinic instability

A dimensionless measure of the vertical temperature contrast, $\sigma_z \Delta T_{\max}$ (see equation (3.2)), is the parameter

$$B \equiv \frac{gd\sigma_z \Delta T_{\max}}{4\Omega^2(b-a)^2} = 0.25\sigma_z \Pi_4 \qquad (4.1)$$

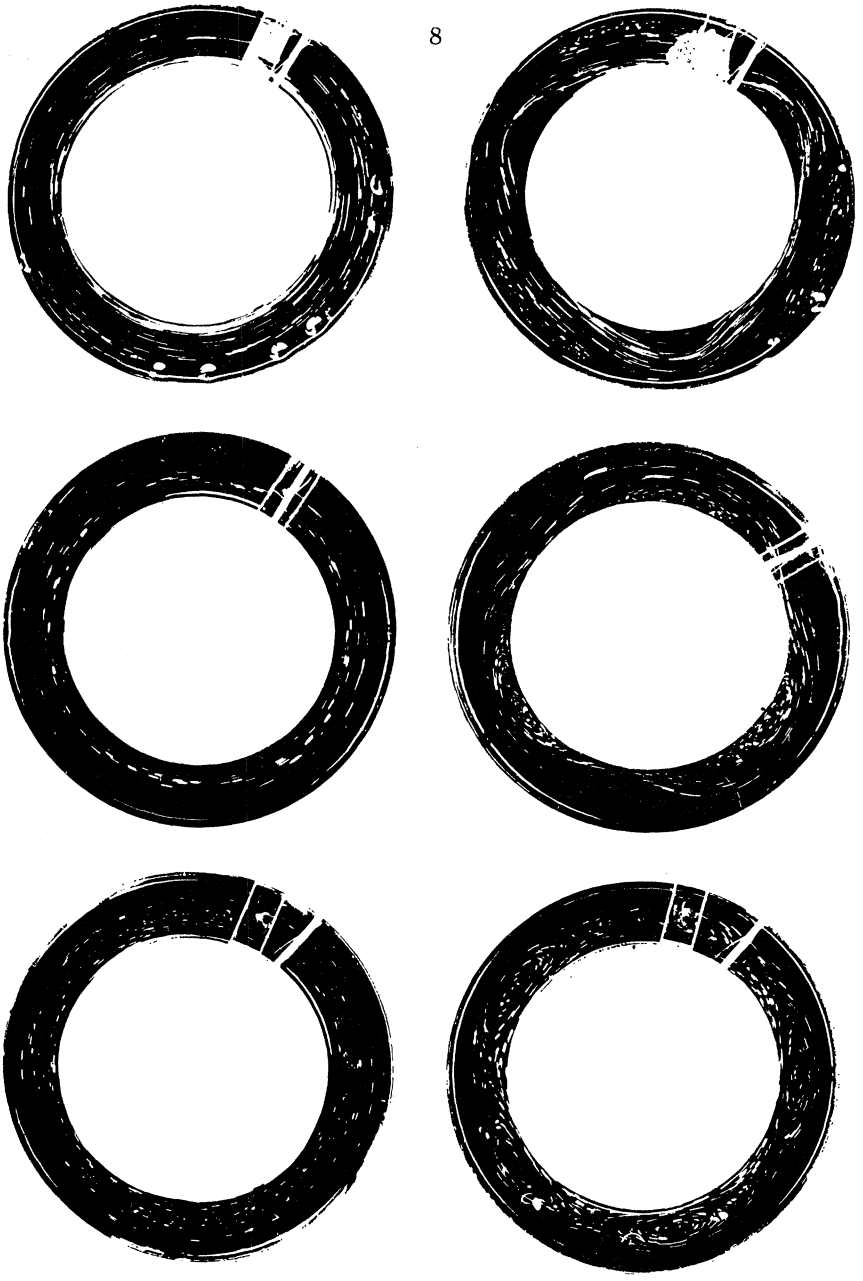

	Ω/rad s^{-1}	P/J s^{-1}		Ω/rad s^{-1}	P/J s^{-1}
(*a*)	1.49	133	(*d*)	1.67	132
(*b*)	0.87	24	(*e*)	1.46	96
(*c*)	0.52	123	(*f*)	1.26	134

FIGURE 8. Streak photographs illustrating the top-surface flow patterns in the symmetric régime (left column) and the steady waves régime (right column) of thermal convection in an internally heated rotating fluid annulus of small gap-width (see also figure 9, cf. figures 6 and 12). The pictures illustrate the dependence of the general characteristics of the flow pattern on the manner by which heat is removed from the system (top row, inner wall cooled; middle row, outer wall cooled; bottom row, both walls cooled), and confirm the theoretical predictions of § 2, as illustrated by figure 3. (Liquid used: water; upper surface: free; basic rotation: anticlockwise; $a = 5.71$ cm, $b = 8.55$ cm, $d = 12.0$ cm.)

(see table 2 and Rev.). B is the central parameter in the theory of baroclinic instability, in terms of which process the 'upper transition' between steady baroclinic waves and axisymmetric flow (see figure 2) in the case of wall-heating has been interpreted with both qualitative and quantitative success (see Rev.). B is an internal dimensionless parameter not, unlike the 'external dimensionless parameter' Π_4 in the case of wall-heating (see table 2), under the direct control of the experimenter. However, as B can be determined more accurately than Π_4 in the case of internal heating, its direct theoretical significance makes it an appropriate and useful parameter to use here in the presentation of experimental results.

One of the principal results of experiments with wall-heating is the remarkable near-independency of σ_z on Ω, a, b, d, etc. throughout most of the axisymmetric and the non-axisymmetric régimes of flow (see Hide 1967); using the present apparatus and method of estimating σ_z we found that this quantity varies between 0.68 and 0.88 over the range of Ω from 0.25 to 4.0 rad s^{-1} (cf. figure 16 and table 3). Within the axisymmetric régime σ_z increases steadily with Ω up to a maximum at the transition to wave flow, where a sharp decrease occurs. Within the non-axisymmetric régimes, variations of σ_z with Ω are less marked and not monotonic. Internally heated systems were found to behave in a generally similar way. Thus, the corresponding ranges of variation of σ_z when the upper surface was free was 0.75 to 0.85 in the case when both side-walls were cooled simultaneously, 0.70 to 0.80 in the case of inner-wall cooling and 0.70 to 0.80 in the case of outer-wall cooling. In the last two cases, the placing of a rigid lid in contact with the upper surface altered the range of σ_z to 0.75 to 0.85.

Experimental determinations of the transition between axisymmetric flow and steady baroclinic waves plotted in a B versus Π_5 diagram are presented in figure 15. The point labelled 'H.K.' was obtained from thermocouple measurements in a very large wall-heated annulus (see Ketchum 1968) and the curve labelled 'F.H.' is based on visual observations of a small wall-heated annulus (see figure 2, also Fowlis & Hide 1965), the conversion from Π_4 to B being made by taking $\sigma_z = 0.8$ (see equation (4.1)). The maximum error in each determination of B at the transition amounted to $\pm 20\,\%$; it was due largely to uncertainties in the variation of $\partial T/\partial z$ with z throughout the fluid. At $\pm 8\,\%$, the corresponding error in Π_5 was small in comparison.

These results indicate that, to within this degree of accuracy, the upper transition is fairly insensitive to the detailed structure of the temperature and velocity fields in the axisymmetric régime. Moreover, the experimental values of B at which the transition occurs agree reasonably well with Eady's theory of small-amplitude baroclinic instability of the simplest-imaginable shear flow in a rotating stratified fluid (see Rev.).

Each determination of B_{crit}, the value of B at the upper transition, was made as follows. From determinations of the form of the upper-surface flow pattern at different values of Ω in a typical experimental run (see § 3 above), in which P was kept fixed, it was possible to find an approximate value of B_{crit} based on the arithmetic mean of the lowest value of Ω at which axisymmetric flow occurred and the highest value of Ω at which waves occurred. This arithmetic mean value was then used as a starting-point for an iterative procedure for determining a more accurate value of B_{crit}, corresponding to that value of Ω at which a 2% change in Ω, in the right direction, brought about a transition from one type of flow to the other. The critical value of Ω found in this way was reproducible to $\pm 5\,\%$; the corresponding reproducibility of B_{crit} was $\pm 10\,\%$.

The exact nature of the transition depends to some extent on ΔT_{max}. At $\Delta T_{\mathrm{max}} \simeq 10$ K and 30 K amplitude vacillation (see Rev.) occurred at the transition. The corresponding amplitude

of the temperature fluctuations recorded by a thermocouple in the convecting liquid, typically $0.2\Delta T_{\max}$ in the wave régime, would fall abruptly at the transition. However, at $\Delta T_{\max} \simeq 4\,\mathrm{K}$ the transition occurred in a somewhat different way; the wave-amplitude as determined visually and from thermocouple traces decreased gradually with decreasing Ω as the axisymmetric régime was approached. The transition point was taken (arbitrarily) as being when the amplitude of the temperature fluctuations had decreased to 0.01 of that found well within the wave régime.

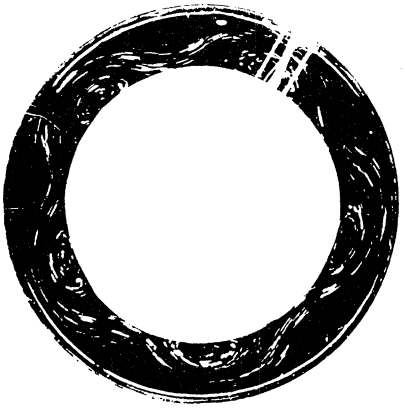

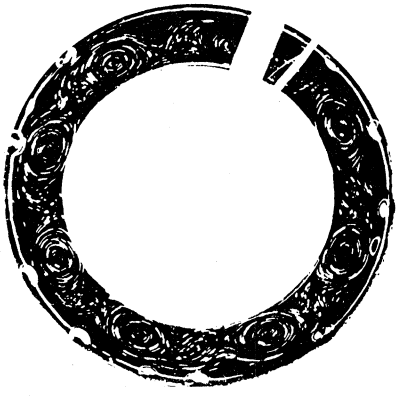

	Ω/rad s^{-1}	P/J s^{-1}		Ω/rad s^{-1}	P/J s^{-1}
(*a*)	2.32	131	(*d*)	3.33	142
(*b*)	1.94	98	(*e*)	4.00	120
(*c*)	2.32	138	(*f*)	3.30	138

FIGURE 9. Streak photographs illustrating top-surface flow patterns in the steady waves régime of thermal convection in an internally heated rotating fluid annulus of small gap-width (see also figure 8, cf. figures 6 and 12). The pictures illustrate how the wavenumber increases with increasing Ω. Top row, inner wall cooled; middle row, outer wall cooled; bottom row, both walls cooled. (Liquid used: water; upper surface: free; basic rotation: anticlockwise; $a = 5.71$ cm, $b = 8.55$ cm, $d = 12.0$ cm.)

Previous work with wall-heated systems (Fowlis & Hide 1965) has shown that the 'lower transition' between axisymmetric and steady wave flow is relatively insensitive to the value of Ω (see figure 2). More precisely, when $T_b > T_a$ the transition occurs when

$$\frac{10^{-4} g \Delta\rho_{\max} (b-a)^3}{\bar{\rho}\nu\kappa} \left(\frac{d}{b-a}\right) \left(\frac{\nu^2}{4\Omega^2 (b-a)^4}\right)^{0.136 \pm 0.043} = 3.5 \pm 2.1,$$

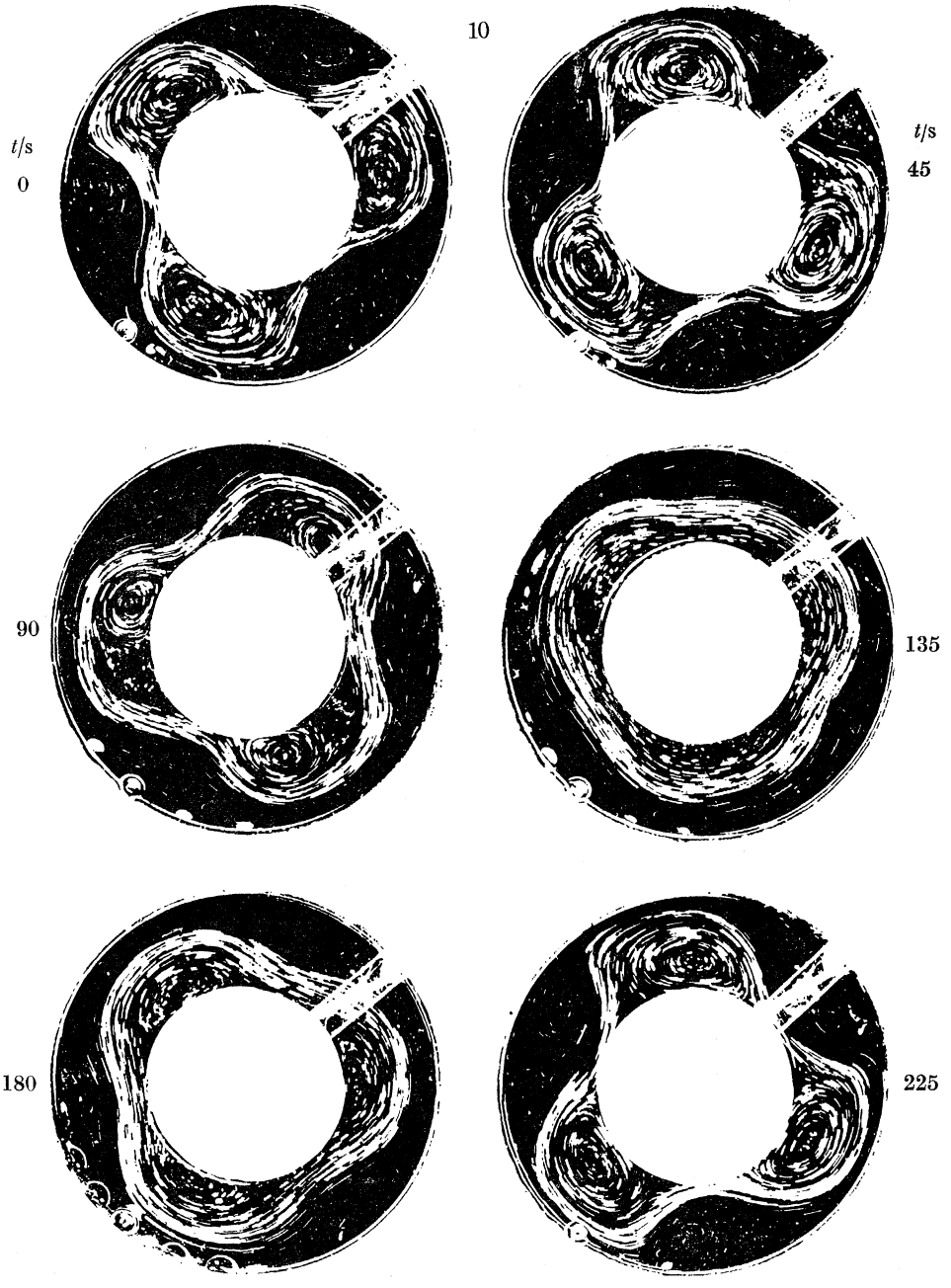

FIGURE 10. Streak photographs illustrating top-surface flow patterns during one cycle of wave-amplitude vacillation in an 'internally heated outer wall cooled' rotating fluid annulus. (Liquid used: water; upper surface: free; basic rotation: anticlockwise; $a = 4.06\,\text{cm}$, $b = 8.55\,\text{cm}$, $d = 12.0\,\text{cm}$, $\Omega = 1.22\,\text{rad s}^{-1}$, $P = 130\,\text{J s}^{-1}$.)

(with complications that we cannot go into here when $T_b < T_a$). The two determinations of the lower transition made in the present experiments with internal heating are based on two runs with an 'inner-wall cooled' system carried out by holding Ω constant at 0.968 or 3.52 rad s^{-1} and

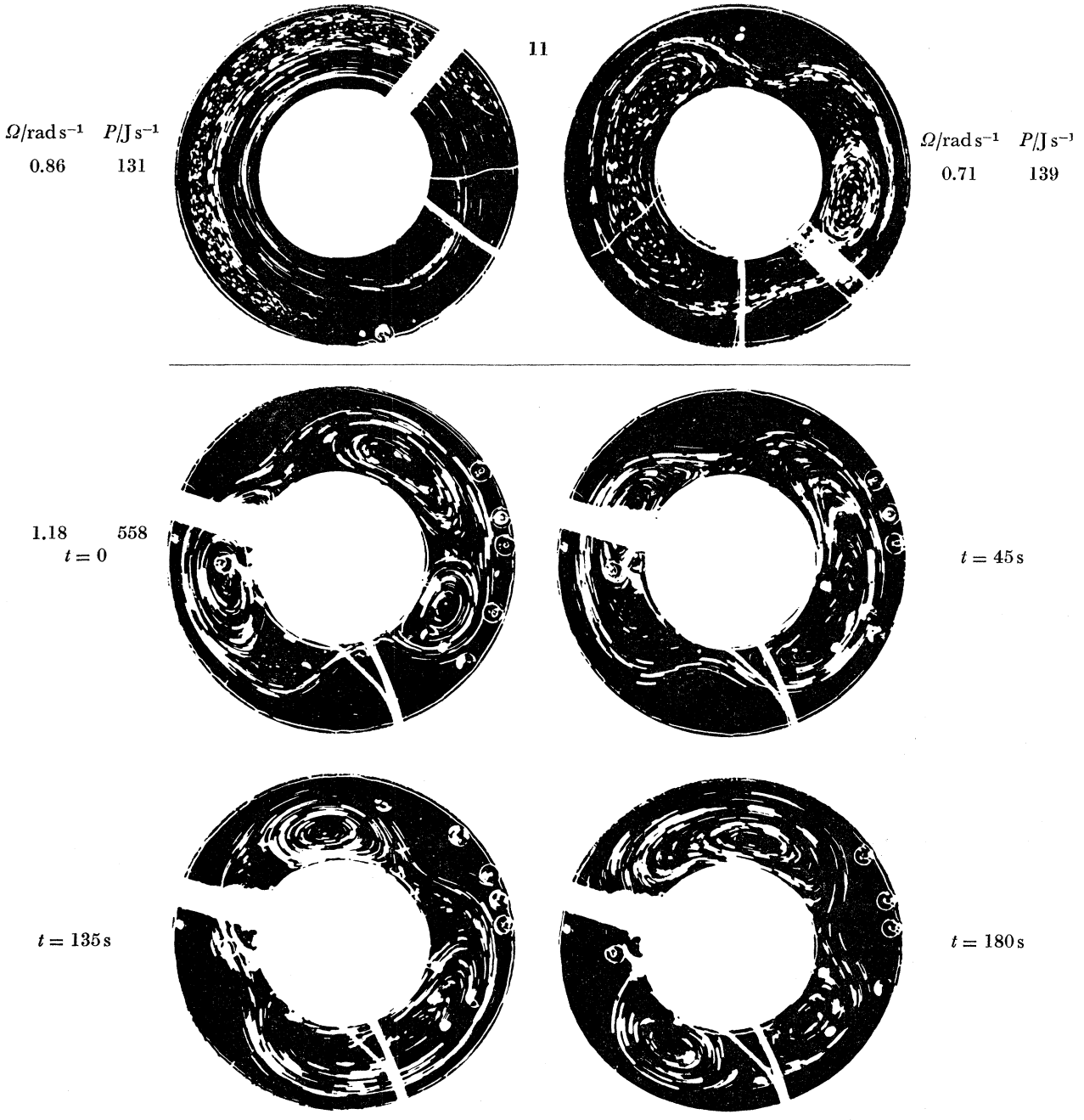

FIGURE 11. Streak photographs illustrating top-surface patterns of regular non-axisymmetric flows, under conditions near to the transition to 'upper' axisymmetric flows, in an internally heated fluid annulus. *Top row*: steady wave with $m = 1$ and inner wall cooled (left picture) and steady but asymmetric wave, outer wall cooled (right picture). *Middle and bottom rows*: Illustrating one vacillation cycle in an example of this phenomenon studied in the 'both walls cooled' case (cf. figure 7 and text). (Liquid used: water; upper surface: free; basic rotation: anticlockwise; $a = 4.06$ cm, $b = 8.55$ cm, $d = 12.0$ cm.)

varying the power input. Remarkably, the values of $\Delta\rho_{\max}$ at the transitions thus determined give, when substituted in the last equation, values of 3.0 and 3.6 for the left-hand side of the last equation.

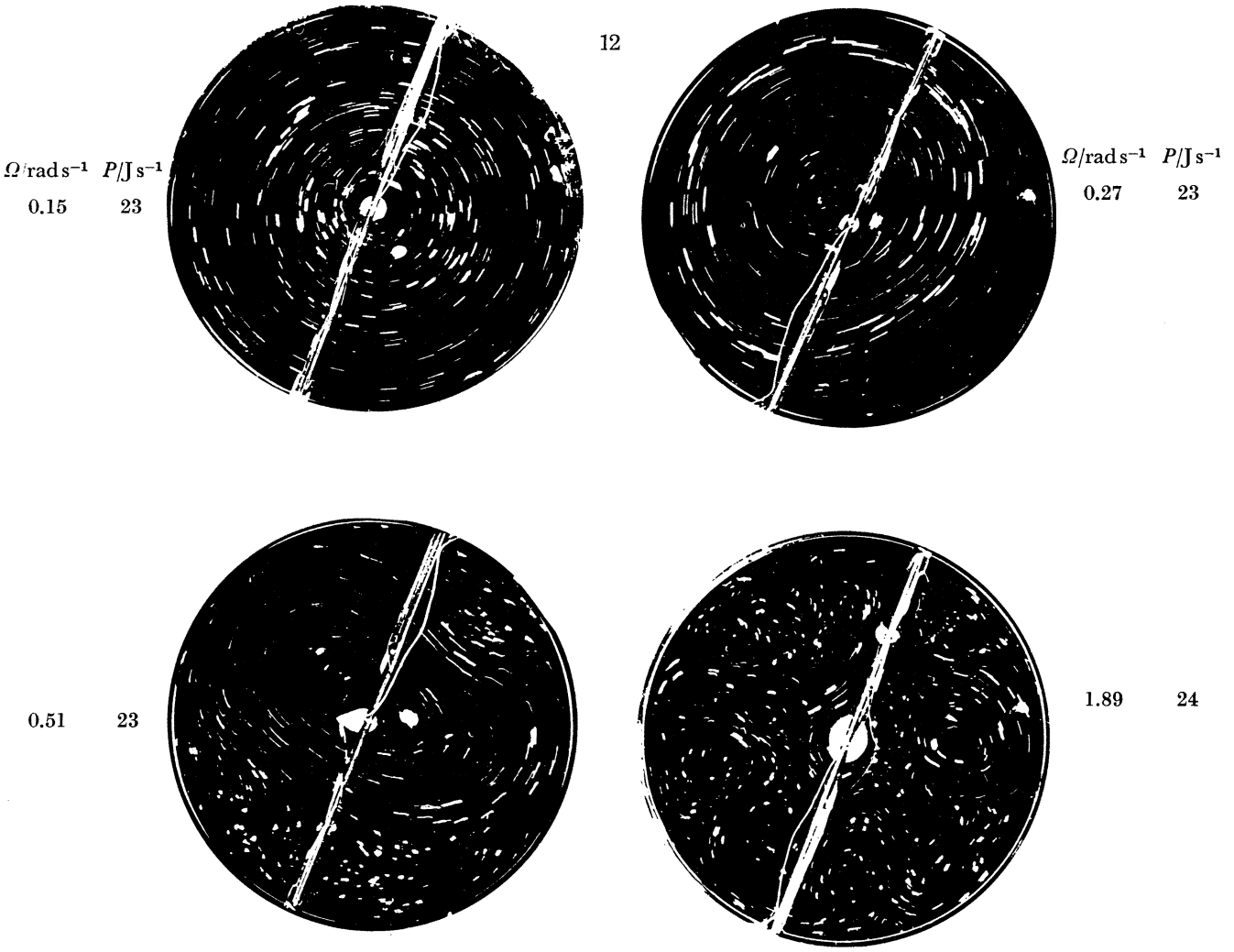

FIGURE 12. Streak photographs illustrating top-surface flow patterns of thermal convection in an internally heated, outer wall cooled rotating fluid annulus of large gap width; $(b-a) \div b$. When $\Omega = 0.15\,\mathrm{rad\,s^{-1}}$ (top left picture) the flow is axisymmetric; at somewhat higher values of Ω, namely $0.27\,\mathrm{rad\,s^{-1}}$ and $0.51\,\mathrm{rad\,s^{-1}}$ (top right and bottom left), steady waves occurred with wavenumbers $m = 1$ and $m = 2$ respectively. Irregular flow occurred at the highest value of Ω, namely $1.89\,\mathrm{rad\,s^{-1}}$ (bottom right). The experiment shows that there is no qualitative difference between the cases $a \ll b$ and $a \not\ll b$ (and refutes a conjecture which has gained widespread acceptance in meteorological circles, namely that steady waves should only be possible when $a \not\ll b$). (Liquid used: water; upper surface: free; basic rotation: anticlockwise; $a = 0.04\,\mathrm{cm}$, $b = 8.55\,\mathrm{cm}$, $d = 12.0\,\mathrm{cm}$.)

(*b*) *Steady waves*

The implications of equation (2.19) with regard to the dependence of the main geostrophic features of fully developed wave patterns on the manner of heating and cooling are indicated schematically in the third column of figure 3.

In the vicinity of a bounding cylinder through which no heat passes ('thermal equator'!) the line-integral of the azimuthal component of geostrophic flow must vanish. This constraint on the shape of the flow pattern requires in the wave régime anticyclonic (at the top surface) eddies

in contact with the 'thermal equator', the outer or inner cylinder as the case may be (cf. figures 3 *c*, *d*). These theoretical predictions accord well with the experimental results presented in figures 6 *d*, 7 *a*, 8 *d*, 9 *a*, *d* and in figures 6 *e*, 7 *b*, 8 *e*, 9 *b*, *e*.

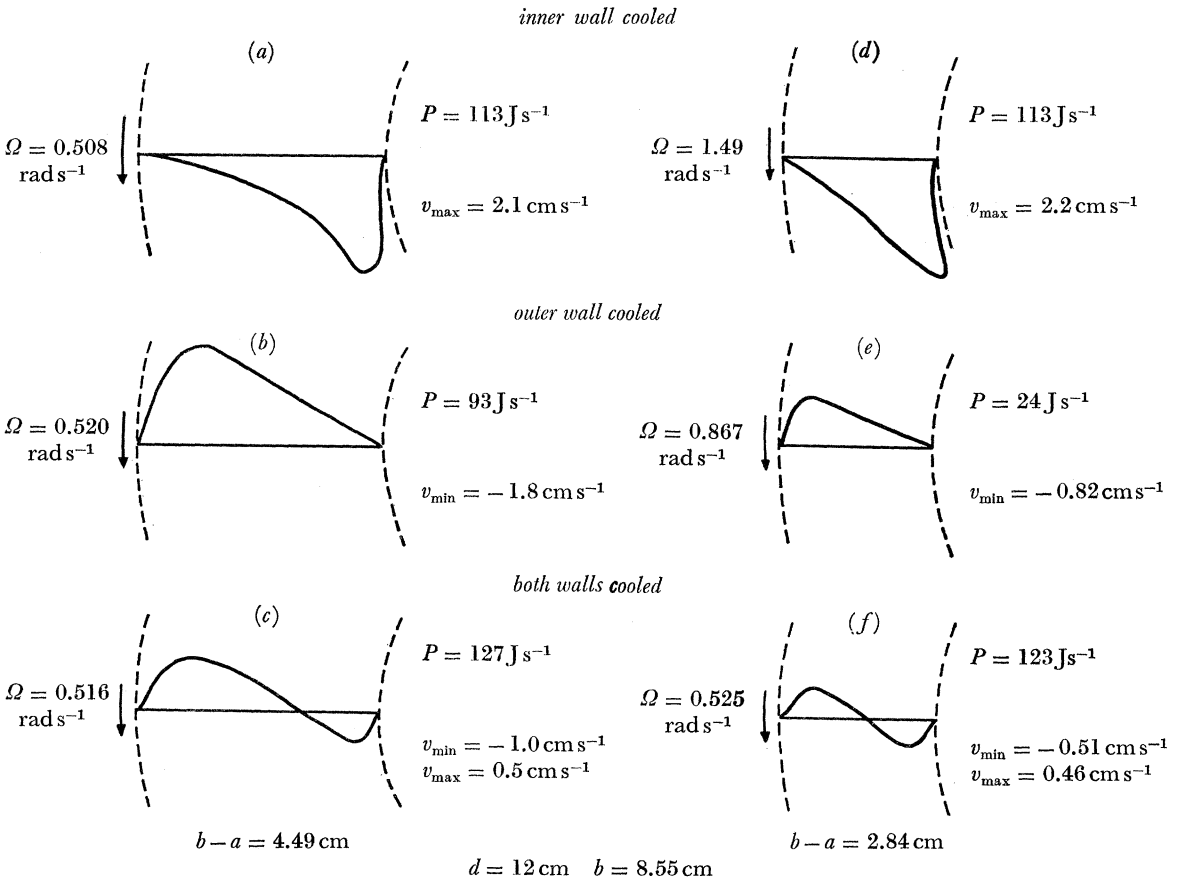

FIGURE 13. Typical profiles of the top-surface azimuthal flow velocity for axisymmetric flows in an internally heated annulus, based on streak photographs (see figures 7).

Likewise, the theoretical prediction illustrated by figure 3 *e* is verified by the results presented in figures 6 *f*, 7 *c*, 8 *f*, 9 *c*, *f*. In this case, heat leaves the system via both inner and outer cylinders, and, according to equation (2.19), the sign of the zonally-averaged azimuthal flow velocity near one bounding cylinder should (in contrast to the cases illustrated by figures 3 *a*, *b*) be opposite to that for the other bounding cylinder.

We must point out that the still photographs presented here are relatively poor representations of what is observed. Direct visual observations (and ciné films) provided most convincing and unambiguous evidence that the arguments presented in § 2 suffice to predict the general features of the fully developed wave-flow pattern.

The effect on the steady-waves régime of varying the distance $b-a$ between the bounding cylinders has been studied extensively for the case of wall heating (see Rev.). The principal findings of these studies in regard to the range of wavenumber m occurring within the steady-waves régime is given roughly (having regard for the fact that m must be an integer) by

$$0.2 < m(b-a)/\pi(b+a) < 0.7 \qquad (4.2)$$

when viscosity is not too important (more precisely, when Π_5 exceeds about twice the critical value below which only axisymmetric flow occurs, see figure 2). The present experiments indicate that equation (4.2) is also valid for internally heated systems (cf. figures 5, 6, 8, 9).

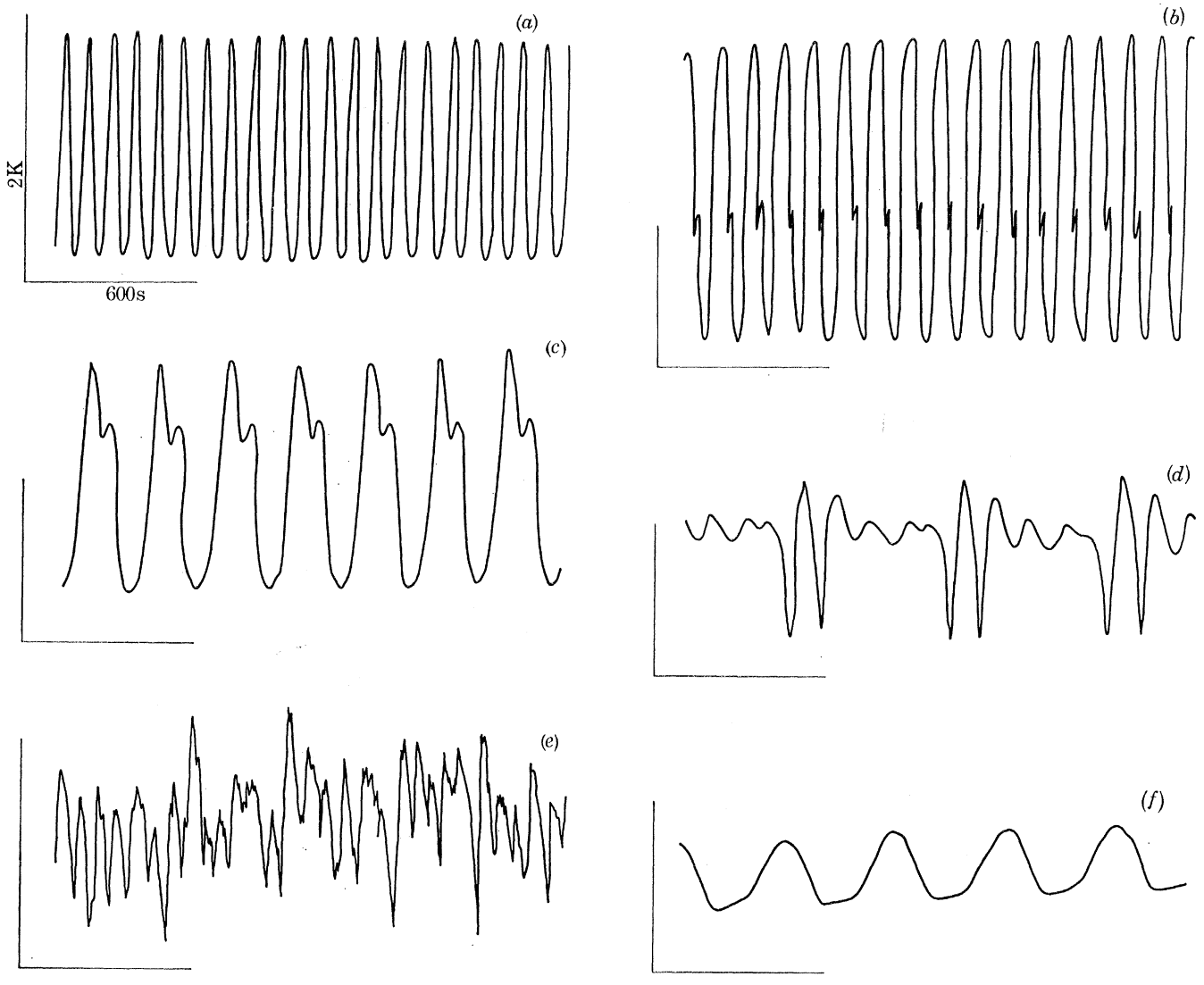

FIGURE 14. Typical temperature against time traces recorded by a thermojunction at a point with coordinates $(r, \phi, z) = (\frac{1}{2}(a+b), 0, \frac{5}{12}d)$, within a rotating fluid annulus subject to internal heating (see figure 4). The length of the line along the time axis (the abscissa) is equivalent to 600 s and that of the line along the temperature axis (the ordinate) to 2.0 K. Traces (*a*) to (*e*) correspond to the same geometry and trace (*f*) to the case of vanishingly small inner cylinder.

Traces (*a*) to (*c*) are typical of steady waves (see figures 6 *d*, *e*, *f*) in the respective cases of cooling at the inner wall, outer wall and both walls. Traces (*d*) and (*e*) respectively are cases of amplitude vacillation (see figure 10) and irregular flow (see figure 7 *e*) when the outer wall is cooled. Trace (*f*) is for the steady wave corresponding to figure 12 *c*. (Some experimental details: $b = 8.55$ cm, $d = 12.0$ cm; liquid used: water; upper surface: free.)

The effect on the steady waves régime of reducing the radius of the inner cylinder to (virtually) zero

The experiment illustrated by figure 12 demonstrates that the (virtual) absence of an inner cylinder does not preclude the occurrence of steady waves, thus refuting a conjecture that seems to have gained widespread acceptance amongst meteorologists (see Rev.). Figure 12 gives streak

photographs illustrating the types of flow obtained when the inner cylinder is a fine copper wire. These photographs show that the axisymmetric, steady-wave, vacillating and irregular flows found when $a \not\ll b$ also occur when $a \ll b$. Moreover, the observed wavenumbers of the regular non-axisymmetric flows, namely $m = 1$ and $m = 2$, are consistent with equation (4.2), an

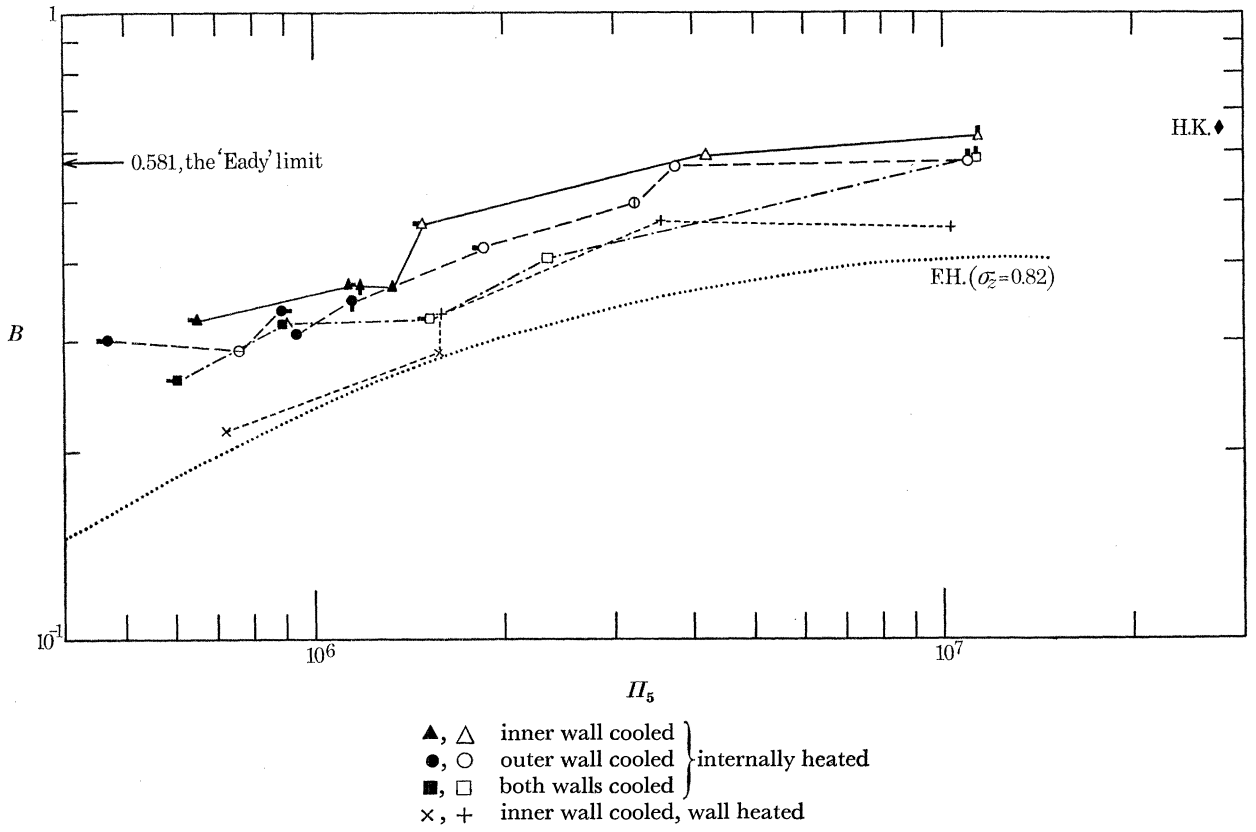

FIGURE 15. Determinations, based on temperature measurements, of the transition between the 'upper symmetrical' and the 'steady waves' régime (see figure 3), plotted in a B ($= 0.25\sigma_z \Pi_4$ see equation (3.2)) versus Π_5 diagram. (The point labelled H.K. was obtained with a very large wall-heated annulus (see Ketchum 1968). The curve labelled F.H. is based on visual observations in a wall-heated annulus (see Fowlis & Hide (1965) and figure 3).) The maximum error in each determination of B at the transition amounted to about $\pm 20\%$. The results indicate that, to within this degree of accuracy, the transition is fairly insensitive to the detailed structure of the temperature and velocity fields in the axisymmetric régime. Moreover, the experimental value of B at which the transition occurs agrees reasonably well with small-amplitude baroclinic instability theory (see text), namely $B = 0.581$ (when $\Pi_5 \to \infty$), although the observed wavenumbers differ significantly from the theoretical values (cf. figure 3). Not plotted in this diagram are two determinations of B and Π_5 at the 'lower transition' with the inner wall cooled, which agree remarkably well with corresponding results in the case of wall-heating when $T_b > T_a$, see figure 2. (See tables 2, 3 and 4 for further experimental details.)

important result in view of its simplicity and intuitive plausibility, notwithstanding the impossibility of accounting for it by means of linear instability theory.

Vacillating as well as steady-wave patterns were observed at $m = 1$. The shape of the $m = 2$ patterns (found at smaller values of B) seemed to waver slightly, but the drift speed, ω, was quite constant.

As determined by visual observation, the 'upper transition' occurred at $B_{\text{crit}} = 1.0 \pm 0.2$, 0.6 being the corresponding value of B_{crit} when $a \not\ll b$. Inasmuch as this increase in the critical

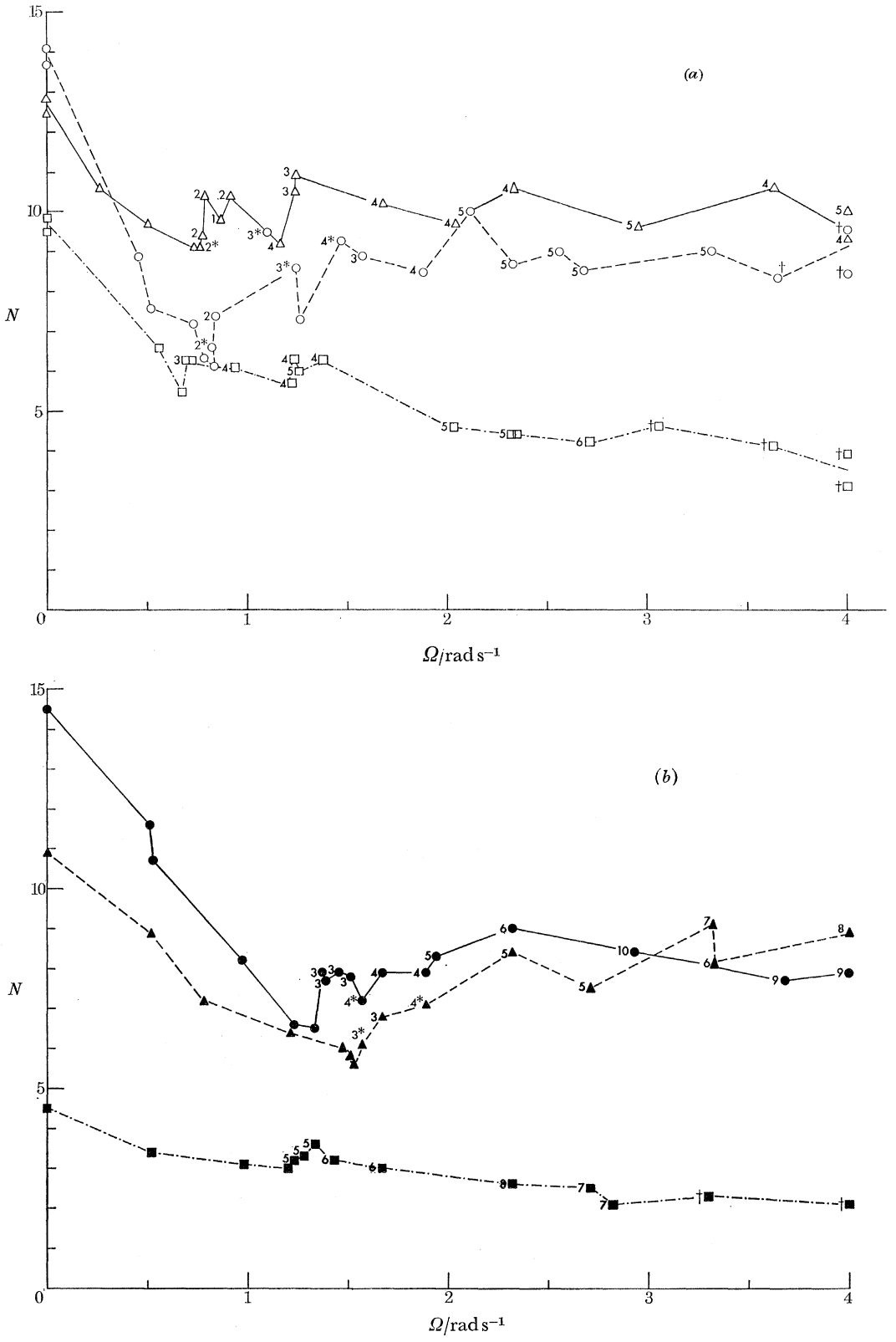

FIGURES 16. Experimental determinations of Nusselt number, N, the heat transfer coefficient (see equation (3.3)) at different values of Ω for an internally heated rotating fluid annulus of width (*a*) $b-a = 4.49$ cm, and (*b*) $b-a = 2.84$ cm (when $|T_b - T_a|$ or $|T_{\sqrt{(ab)}} - T_a| = 10$ K, see equations (3.5) and (3.6)). The wavenumber m is given with each point; where no number is given the flow was axisymmetric. Amplitude vacillation indicated by * irregular flow by †. The small corrections required to reduce each observation to the same value of the impressed temperature contrast, namely 10 K, were based on experimental determinations of the (slow) dependence of N on that temperature contrast. For the sake of clarity error bars on N are not given in the diagram; they amounted to $\pm 10\%$ (see text). Key:

△ or ▲ inner wall cooled
○ or ● outer wall cooled
□ or ■ both walls cooled.

(See table 4 for further experimental details.)

value of B can be attributed to curvature effects, it accords fairly well with theoretical expectation based on a comparison between work of Davies and Eady (see Rev.).

Heat flow, temperature variations and drift speeds

The heat-flow determinations plotted in figures 16 are generally consistent with those found with wall-heated systems, where the dependence of Nusselt number N on Ω within the steady-waves régime is much weaker than in the axisymmetric and irregular régimes, and not even monotonic (see Rev.). When comparing the different cases it is worth remembering that for given $\Delta T_{\max}$ (see equation (3.2)), heat transfer in the 'corresponding conductive state' for the case when both walls are cooled exceeds by a factor of 4 that for the case when only one wall is cooled.

Figures 14 *a*, *b*, *c*, *e* are typical temperature against time traces recorded by a thermojunction at a point with coordinates $(r, \phi, z) = (\frac{1}{2}(a+b), 0, \frac{5}{12}d)$, see figure 4. The oscillatory variations are due to the steady drift of the system of steady-waves with angular velocity ω relative to the rotating apparatus.

Determinations of ω for internally heated systems are plotted in figures 17, where the ordinate is a dimensionless quantity,

$$10^2\omega/\Omega\Pi_1\Pi_4. \tag{4.2}$$

This quantity was found in the original experiments with wall-heating to lie between 2.4 and 3.4, and $\frac{1}{2}(a+b)\,\omega$ was interpreted as the average value of the relative azimuthal velocity v throughout the fluid, a result which accords well with baroclinic instability theory (see Rev.). This rough interpretation of ω is generally consistent with the corresponding results for the case of internal-heating presented in figure 17, as evinced by the magnitude and sign of the ordinate, but without accurate determinations of v at many points within the fluid the interpretation cannot be tested precisely.

In the case of cooling at both walls (see figure 17 *c*), symmetry considerations indicate that ω should vanish except in so far as effects due to curvature of the side-walls and, to a lesser extent, to variations of viscosity with temperature, cannot be neglected. Curvature effects probably account for the difference seen in figure 17 *c* between the sets of points corresponding to different gap widths. It is not quite clear why when one wall only is cooled, the variation of the ordinate with Ω should be more marked when it is the outer wall that is cooled than when it is the inner wall (compare figures 17 *a*, *b*).

The effect on ω of placing a rigid lid in contact with the upper surface is a considerable reduction in magnitude, by more than a factor of 10, in keeping with expectation based on symmetry considerations. The non-vanishing of ω in this case is probably due to non-uniformity of ν due to the dependence of ν on T.

(*c*) *Vacillating and irregular flows*

Vacillation

Figure 10 comprises a sequence of streak photographs of top-surface flow patterns during one cycle of a typical example of wave-amplitude vacillation (see Rev.) in an internally heated annulus when the outer wall is cooled; figure 14 *d* is a corresponding temperature trace. As with steady waves (cf. figure 6 *e*), the flow pattern is characterized by the presence of intense anti-cyclonic eddies in contact with the inner cylinder, in addition to the wavelike meandering jet. Amplitude vacillation is evidently not restricted to the vicinity of the upper transition but it

seems to be most pronounced there. With one side-wall cooled the phenomenon occurred in runs with $\Delta T_{\max} \approx 13$ and 40 K but not when $\Delta T_{\max} \approx 4$ K; with both walls cooled it occurred only when $\Delta T_{\max} \approx 40$ K and had the form illustrated in the second and third rows of figure 11.

Irregular flow

The transition from steady-waves to irregular flow (see figure 2) is typically more gradual than that between steady waves and axisymmetric flow (see § 4 (*a*)) and is therefore more difficult to

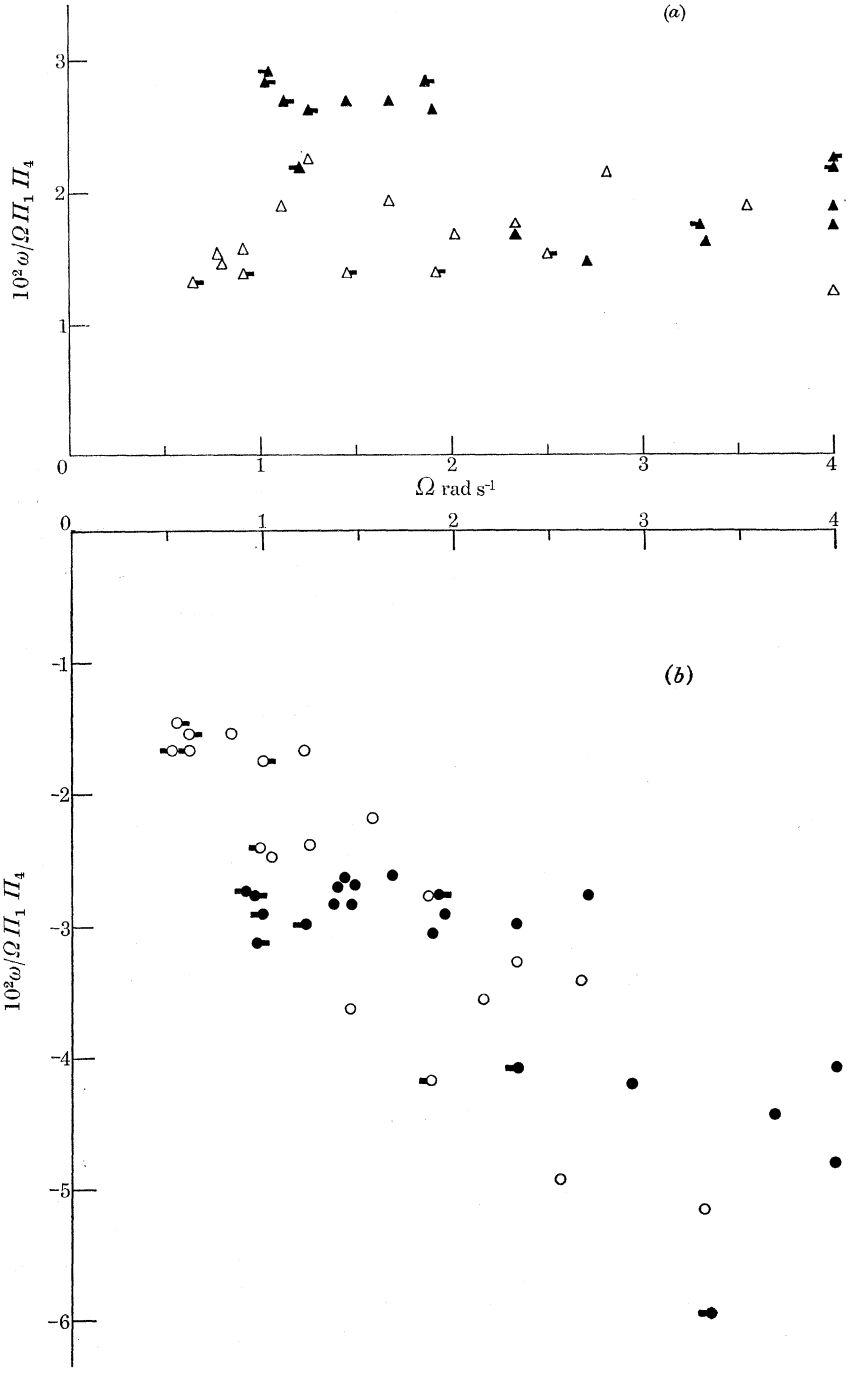

FIGURE 17 (*a*) and (*b*). For legend see facing page.

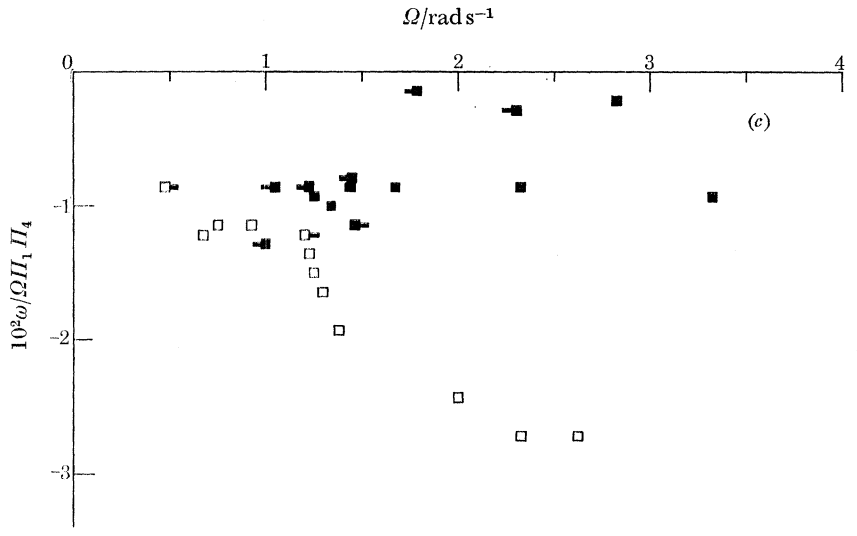

FIGURES 17. Determinations of the drift angular velocity, ω rad s^{-1}, of steady waves in an internally heated rotating fluid annulus when (*a*) the inner wall, (*b*) the outer wall and (*c*) both walls were cooled. The key to the symbols is given in table 4. In the original experiments with wall heating (see Rev.), the ordinate $10^2\omega/\Omega\Pi_1\Pi_4$ was found to lie between 2.4 and 3.4 and $\frac{1}{2}(b+a)\omega$ was interpreted as the average value of the azimuthal flow velocity v throughout the fluid.

TABLE 4. KEY TO SYMBOLS USED IN FIGURES 15, 16 AND 17

inner wall cooled	outer wall cooled	both walls cooled	$\frac{b-a}{\text{cm}}$	range of $\Delta T_{\max}$ / K	$\frac{d}{\text{cm}}$	upper surface
internal heating						
▲	●	■	4.49†	37–42	12	free
△	○	□	4.49†	12–16	12	free
▲	●	■	4.49†	3–4	12	free
▲	●	■	2.84†	12–16	12	free
▲	●	■	2.84†	3–4	12	free
▲	●	■	2.84†	12–16	6	free
▲	●	■	2.84†	12–16	12	rigid
	⊖		3.49‡	12–16	12	free
wall heating						
+			4.49†	3–4 12–16 37–42	12	free
	×		2.84†	3–4 12–16	12	free

† Both side walls copper. ‡ Cold side wall copper, warm side wall Perspex.

PHILOSOPHICAL TRANSACTIONS OF THE ROYAL SOCIETY A MATHEMATICAL, PHYSICAL & ENGINEERING SCIENCES

define either in terms of visual observations or of the form of thermocouple traces (see figure 14). From runs at different values of $b-a$ and $\Delta T_{\max}$ (the corresponding range of Π_5 being 10^7 to 10^8), the following information on the transitional ranges of B was deduced:

inner wall cooled:	$< 0.03 \pm 0.01$	to	$> 0.02 \pm 0.01$,
outer wall cooled:	$< 0.04 \pm 0.01$	to	$> 0.03 \pm 0.01$,
both walls cooled:	$< 0.08 \pm 0.01$	to	$> 0.05 \pm 0.02$.

These values are comparable with those found for wall-heated systems over the same range of Π_5.

References

Fowlis, W. W. & Hide, R. 1965 *J. Atmos. Sci.* **22**, 541–558.
Hide, R. 1958 *Phil. Trans. Roy. Soc. Lond.* A **250**, 442–478.
Hide, R. 1967 *Phys. Fluid.* **10**, 56–68.
Hide, R. 1970 In *The global circulation of the atmosphere* (ed. G. A. Corby, pp. 196–221). London: Royal Meteorological Society. (Cited as 'Rev.')
Lorenz, E. N. 1967 *World Meteorol. Organizn* Publ. no. 218 (161 pages).
Kaiser, J. A. C. 1969 *Tellus* **21**, 789–805.
Ketchum, C. B. 1968 Ph.D. thesis, Massachusetts Institute of Technology.
Ward, F. W. 1965 *Astrophys. J.* 141, 534–547.

PHILOSOPHICAL TRANSACTIONS OF THE ROYAL SOCIETY A MATHEMATICAL, PHYSICAL & ENGINEERING SCIENCES

	Ω/rad s^{-1}	P/J s^{-1}
(*a*)	1.22	122
(*b*)	1.23	90
(*c*)	1.22	129
(*d*)	3.98	129
(*e*)	3.98	90
(*f*)	3.98	142

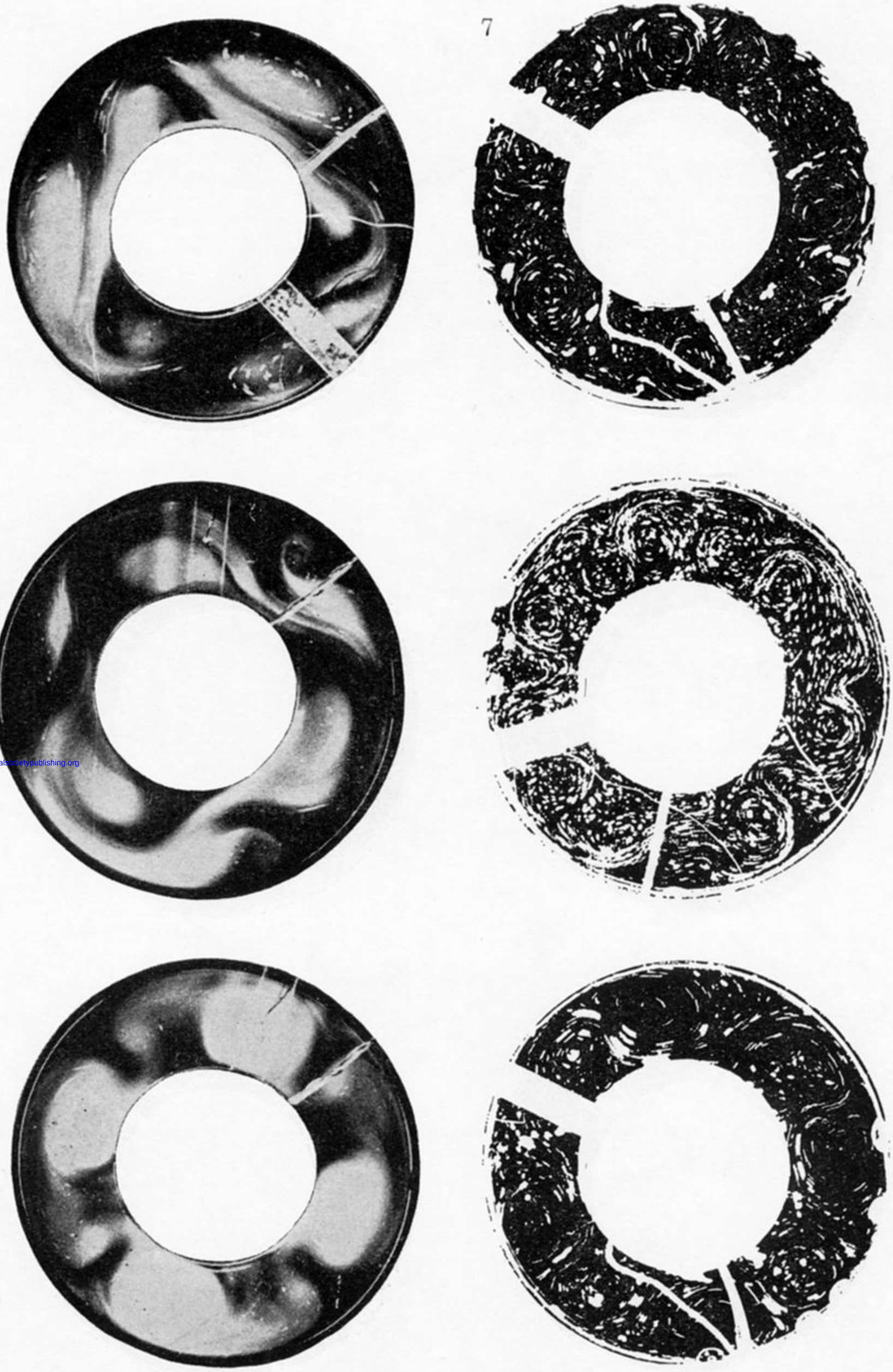

FIGURE 7. Further photographs illustrating top-surface flow patterns in an internally heated rotating fluid annulus. The first column shows the appearance of the steady-wave flows illustrated by the second column of figure 6 when aluminium powder in suspension is used as the flow-visualization technique. The second column consists of streak photographs of the irregular waves that occur at somewhat larger values of Ω. Top row, inner wall cooled; middle row, outer wall cooled; bottom row, both walls cooled. (Liquid used: water; upper surface: free; basic rotation: anticlockwise; $a = 4.06$ cm, $b = 8.55$ cm, $d = 12.0$ cm.)